JAERI-M
87-161

REVIEW : STUDY OF SINGLE-PELLET INJECTION EXPERIMENTS AND DEVELOPMENT OF PELLET INJECTOR IN JFT-2M

October 1987

Satoshi KASAI, Yukitoshi MIURA, Kouichi HASEGAWA
and Seio SENGOKU

日 本 原 子 力 研 究 所
Japan Atomic Energy Research Institute

JAERI-Mレポートは，日本原子力研究所が不定期に公刊している研究報告書です。
入手の問合わせは，日本原子力研究所技術情報部情報資料課（〒319-11茨城県那珂郡東海村）あて，お申しこしください。なお，このほかに財団法人原子力弘済会資料センター（〒319-11 茨城県那珂郡東海村日本原子力研究所内）で複写による実費頒布をおこなっております。

JAERI-M reports are issued irregularly.
Inquiries about availability of the reports should be addressed to Information Division Department of Technical Information, Japan Atomic Energy Research Institute, Tokai-mura, Naka-gun, Ibaraki-ken 319-11, Japan.

編集兼発行　日本原子力研究所
印　　刷　いばらき印刷㈱

JAERI-M 87-161

Review : Study of Single-Pellet Injection Experiments and Development of Pellet Injector in JFT-2M

Satoshi KASAI, Yukitoshi MIURA, Kouichi HASEGAWA
and Seio SENGOKU

Department of Thermonuclear Fusion Research
Naka Fusion Research Establishment
Japan Atomic Energy Research Institute
Naka-machi, Naka-gun, Ibaraki-ken

(Received September 12, 1987)

The single pellet injector developed for JFT-2M and the improvement of plasma characteristics in the auxiliary-heated discharges by single-pellet injection are reviewed for the period 1982-1986. The pellet injector is a pneumatic type and the designed pellet size is 1.65 mmϕ × 1.65 mmL and 1 mmϕ × 1 mmL. The hydrogen, deuterium and mixed (H_2+D_2) pellets can be produced with good reproducibility. Maximum pellet velocity is about 970 m/s (pellet is deuterium and propellant gas is hydrogen). In the pellet injection experiments into auxiliary-heated (NB, ICRF) divertor or limiter discharges, the plasma confinement time is improved by a factor of 1.4-1.7 compared with the confinement time in the Ohmic discharges. The achieved confinement time is longer than that on the high confinement mode (H-mode) in gas fueled discharges, although the phenomena are transient.

Keywords: Solid Pellet, Pellet Injector, Pellet Diagnostics, Plasma Confinement, L- and H-modes, Neutral Beam Heating, Ion Cyclotron Range of Frequency Wave Heating, Single-Null Divertor, Tokamak

JAERI－M 87－161

JFT－2Mにおける固体ペレット（Single－Pellet）入射実験及びペレット入射装置開発に関するまとめ

日本原子力研究所那珂研究所核融合研究部
河西　敏・三浦　幸俊・長谷川浩一・仙石　盛夫

（1987年9月12日受理）

本報告書は，昭和57年から昭和61年度に渡って実施した高性能トカマク開発試験装置（JFT－2M）用の1ペレット入射装置の開発と第2段加熱プラズマに高速の固体ペレット（H_2またはD_2）を入射して実現したプラズマ特性の改善に関する実験についてまとめたものである。JFT－2M用に開発したペレット入射装置は，圧縮気体の膨張を利用してペレットを銃身内で加速するニューマチック方式を採用している。生成されるペレットの大きさは，直径1.65 mm，長さ1.65 mmと直径1 mm，長さ1 mmである。この装置では水素，重水素および混合（$H_2 + D_2$）ペレットのいずれをも生成することができる。ペレットの最大射出スピードは，約970 m／s である。中性粒子（NB）入射あるいはイオンサイクロトロン周波数帯（ICRF）波加熱したダイバータ配位あるいはリミター配位のプラズマへペレットを入射した実験を行った。その結果，粒子をガスパフ補給法により行ったときに得られる通常の閉込めモード（Lモード）にペレットを入射すると，NB及びICRF加熱のいずれにおいてもエネルギー閉込め時間が大幅に改善（ガスパフ補給法において得られる高閉込めモード（Hモード）における閉込め時間の1.4－1.7倍）される放電モードを見出した。またICRF加熱におけるHモードにペレットを入射した場合にも同程度の閉込めの改善が見られた。以上の実験結果から，固体ペレットによる粒子補給法がプラズマの性能向上に極めて有効であることが実証された。

那珂研究所：〒311－02 茨城県那珂郡那珂町大字向山801－1

Contents

1. Introduction 1
2. Pellet Injector System 3
2.1 Single-pellet injector 3
2.2 Diagnostic apparatuses of pellet 4
3. Production and Injection of Pellet 6
3.1 Condition of pellet production 6
3.2 Result of pellet injection test 7
4. Experimental Results of Pellet Injection into Plasmas 10
4.1 Pellet injection in NB heated single-null divertor discharges 10
4.2 Pellet injection in the ICRF heated single-null divertor discharges 12
4.3 Pellet injection in the NB + ICRF heated limiter discharges 14
5. Summary and Future Plan 15
Acknowledgements 17
References 18

目　　次

1. 序　　文 …… 1
2. ペレット入射装置 …… 3
2.1　1ペレット入射装置 …… 3
2.2　ペレット診断機器 …… 4
3. ペレットの生成と射出 …… 6
3.1　ペレット生成条件 …… 6
3.2　ペレット射出試験 …… 7
4. プラズマへのペレット入射実験 …… 10
4.1　NB加熱したシングル・ヌル・ダイバータ配位プラズマへのペレット入射 …… 10
4.2　ICRF加熱したシングル・ヌル・ダイバータ配位プラズマへのペレット入射 …… 12
4.3　NB＋ICRF加熱したリミター配位プラズマへのペレット入射 …… 14
5. まとめと将来計画 …… 15
謝　　辞 …… 17
参考文献 …… 18

1. Introduction

Fueling is one of the critical requirements of operating a tokamak fusion reactor in a long pulse or quasi-steady state mode (burn time is long compared to particle confinement time). The solution of this problem, as well as those of providing adequate pumping or exhaust and adequate impurity control, is essential to long pulse operation. Tokamak fusion systems are characterized by small fractional burn up of the fuel and consequently most of the fuel requirement is to meet the particle transport loses from the confinement region.

Injection of a high-speed hydrogen isotope pellet is being considered as a means for fueling future fusion power reactors of the tokamak type. This technique differs from cold-gas inlet at the plasma boundary (i.e. gas puffing). It allows most flexible plasma density profile maintenance as a results of fresh fuel being deposited directly on the innermost flux surfaces. In a future reactor with D-T burn, tritium inventory on the wall is very important problem, which must be solved. The high speed pellet injection should be expected to decrease the tritium inventory on the vacuum chamber wall and the limiter, because the pellet will be well burned.

Fueling experiments with a solid hydrogen or deuterium pellet have been performed in many tokamaks, e.g. ISX[1], Alcator-C[2], TFR[3], PDX[4], PLT[5], ASDEX[6], DIII[7], TFTR[8] and JET[9], to study possibility of improvement of plasma characteristics. Especially, in Alcator-C, a plasma with high electron density ($\bar{n}_e$) and high $n_e(0)\tau_E$ has been produced by pellet fueling ($n_e(0)$: electron density at a plasma center, τ_E: global energy confinement time). Achieved $n_e(0)\tau_E$ = $(0.6 - 0.8 \times 10^{20}$ sec$\cdot$m$^{-3})$ reached the Lawson criterion[2]. The results of pellet injection on TFTR[8] with a large size of a plasma and high temperature have indicated that confinement within the plasma core was improved and the Murakami factor ($\bar{n}_e R/B_t$) obtained with pellets exceeded that which had been achieved by deuterium gas puffing. In JET[9] Ohmic heated discharges, the operational regime is extended by large pellet injection (density limit exceeds by a factor of 2), and increment of electron and ion temperatures is observed in pellet fueled ICRF heating.

In JFT-2M[10], the pellet injection study has been proposed in 1981. Main objects of pellet injection experiments are as follows.

(1) Improvement of plasma parameters in limiter and divertor

configurations (extension of plasma operational regime).

(i) production of high density plasmas (increasing of density limit or improvement of Murakami factor)

(ii) improvement of energy and particle confinements

(iii) production of high-beta plasmas

(iv) control of a plasma density (plasma pressure) profile

(2) Improvement of heating efficiency on the neutral beam (NB) injection and ion cyclotron range of frequency (ICRF) wave heatings.

(3) Identification of particles (thermal electron, runaway electron, fast ion et al.) mainly contributed to the pellet ablation ---- ablation mechanism.

Also, the development of a pellet injector is as follows.

(1) Development of a pellet injector with high-velocity to hyper-velocity.

(2) Improvement of reproducibility of pellet velocity and size of pellet.

(3) Production of H_2, D_2 and mixed (H_2+D_2) pellets.

(4) Development of a multi-pellet injector.

(5) Development of a transfer technique of pellets from the injector to tokamak machine.

Lastly, the possibility of pellet fueling to the large tokamak machine will be found, that is, scaling of pellet fueling to a large machine will be studied.

A fundamental form of an injector has been developed in collaboration with Mitsubishi Atomic Power Industries Inc. in 1982[11]. In the next year, the single pneumatic-gun type injector (pellet size in the carrier: 1 mmϕ × 1 mmL) for JFT-2M was constructed[10]. In Ohmic heated plasmas, electron density rise of about 0.7×10^{19} m^{-3} by this pellet was obtained. And after that, the large pellet (hole size in the carrier is 1.65 mmϕ × 1.65 mmL) has been used on experiments[10]. Up to now, maximum line averaged electron density rise of about 4.5×10^{19} m^{-3} was achieved and significant improvements of energy and particle confinements were performed in Ohmic and auxiliary-heated (NB, ICRF) plasmas with a pellet fueling[12]. In these discharges, electron and ion temperatures near a plasma center gradually recovered for about 30-40 ms after pellet injection, and the rise of radiation loss power (including the charge exchanged particle loss) and level of loss power are relatively low. It is necessary to optimize the timing of pellet injection during

auxiliary heating in order to get an improvement of confinement. Pellets can penetrated deeper in ICRF heating than in NB heating[10].

This paper is the review of the experimental results with pellet injection and the single-pellet injector developed for JFT-2M from 1982 to 1986. In the next section, a pellet injector system and diagnostic apparatuses are described, and some tested fundamental parameters (pellet velocity, mass, pellet shape, pellet ablation, et al.) are presented in section 3. In section 4, the improved confinement results by pellet injection are reviewed and in the last section, obtained results are summarized and the future plan is described.

2. Pellet Injector System[10]

2.1 Single-pellet injector

The pellet injector for JFT-2M is basic type developed at Oak Ridge National Laboratory (ORNL). Figure 1 is the schematic diagram of a single pneumatic pellet injector, which indicates the principle of the injector. A stainless-steel gun barrel (two barrels were prepared: 1 mm bore × 18 mm long and 1.69 mm bore × 18 mm long) is fixed within the barrel housing made of oxygen free copper (OFC) as shown in Fig. 2. A disk shaped stainless steel pellet carrier is situated between the barrel housing and the OFC main housing. The carrier has two holes drilled opposite each other extending through the face of the disk within which pellets are located. A diameter of the hole in one carrier is 1 mm and that 180° by a pulse motor to transport the pellet at the position in an injection line with the gun barrel. The gun assembly is convectively force-cooled by liquid helium. The pellet is propelled from the mechanism by pressurized helium or hydrogen gas. Working pressure of propellant gas is selected to any value from 0 to 30 kg/cm^2.

The primary function of the pellet injection line is to isolate the JFT-2M vacuum vessel from the pellet injector. This is accomplished by using a gas delay line as shown in Fig. 3, which consists of the three vacuum chambers and two stainless steel pipes (an inner diameter is 4 mm and 10 mm). The first chamber (low vacuum chamber) has a mechanical booster pump (pumping speed: 500 m^3/h) and the second chamber (high

auxiliary heating in order to get an improvement of confinement. Pellets can penetrated deeper in ICRF heating than in NB heating[10].

This paper is the review of the experimental results with pellet injection and the single-pellet injector developed for JFT-2M from 1982 to 1986. In the next section, a pellet injector system and diagnostic apparatuses are described, and some tested fundamental parameters (pellet velocity, mass, pellet shape, pellet ablation, et al.) are presented in section 3. In section 4, the improved confinement results by pellet injection are reviewed and in the last section, obtained results are summarized and the future plan is described.

2. Pellet Injector System[10]

2.1 Single-pellet injector

The pellet injector for JFT-2M is basic type developed at Oak Ridge National Laboratory (ORNL). Figure 1 is the schematic diagram of a single pneumatic pellet injector, which indicates the principle of the injector. A stainless-steel gun barrel (two barrels were prepared: 1 mm bore × 18 mm long and 1.69 mm bore × 18 mm long) is fixed within the barrel housing made of oxygen free copper (OFC) as shown in Fig. 2. A disk shaped stainless steel pellet carrier is situated between the barrel housing and the OFC main housing. The carrier has two holes drilled opposite each other extending through the face of the disk within which pellets are located. A diameter of the hole in one carrier is 1 mm and that 180° by a pulse motor to transport the pellet at the position in an injection line with the gun barrel. The gun assembly is convectively force-cooled by liquid helium. The pellet is propelled from the mechanism by pressurized helium or hydrogen gas. Working pressure of propellant gas is selected to any value from 0 to 30 kg/cm^2.

The primary function of the pellet injection line is to isolate the JFT-2M vacuum vessel from the pellet injector. This is accomplished by using a gas delay line as shown in Fig. 3, which consists of the three vacuum chambers and two stainless steel pipes (an inner diameter is 4 mm and 10 mm). The first chamber (low vacuum chamber) has a mechanical booster pump (pumping speed: 500 m^3/h) and the second chamber (high

vacuum chamber) has a turbo-molecular pump (pumping speed: 100 ℓ/s). The last chamber (drift chamber) is evacuated by a 100 ℓ/s turbo-molecular pump. In addition, fast magnetic gate valves (VACOA model: SOV-050-05-SS), situated between the first and second chambers and between the second and last chambers, close behind the pellet for trapping most of the gas in the first and second chambers. The injection line of a pellet makes an angle of about 5.2° with the major radius of the torus in JFT-2M (Fig. 4).

2.2 Diagnostic apparatuses of a pellet

2.2.1 Pellet velocity

A pellet velocity is measured by a pair of photo-interruptors, which consist of a photo-diode (Bell & Howell: Silicon-pin diode 509-01) with IR filter and a light emission diode (Toshiba: GaAs emission diode TLN105). A pair of photo-interruptors, which are installed in the vacuum chamber, are put on the injection line separated by a distance of 1 m (Fig. 5).

2.2.2 Pellet mass

A pellet mass is periodically monitored from the pressure rise by trapping and evaporating the pellet in the chamber (drift chamber). A pressure sencer is a diaphragm type (MKS Instruments Inc.: Baratron 222BHS-BB10). The number of atomic particles can be calculated by the following equation.

$$N_{H,D} = 1.9307 \times 10^{22} \; P_d V_d / T \; ,$$

where P_d(Torr) is pressure rise in the chamber, V_d(ℓ) = 4.98 ℓ (volume of the drift chamber) and T(°K) = 300°K. This method can not be used during the injection experiments into a plasma.

Another method monitored a pellet mass on shot to shot of discharges was developed, which employs a microwave cavity operating at around 8.8 GHz [13]. The microwave cavity is cylindrical, 26 mm in inner diameter and 35.5 mm in inner length. This shows a strong resonance at

8.8 GHz. The mode is the TM_{010}. Q factor of the cavity is about 3175. The change in resonant frequency by a pellet, dielectric sample, is given by

$$|f_o| = 11.1\ f_o P m_p/(MV_c)$$

where f_o is the unperturbed resonant frequency, P is the molar polarisability of a pellet (1.99 cm/mol for deuterium), M is the molecular weight (4 g/mol for deuterium), V_c is the cavity volume (1.9×10^{-5} m^3) and m_p is the pellet mass.

The output signal of the reflected wave generated by the frequency shift as the pellet is travelling in the cavity is detected with the system as shown in Fig. 6.

2.2.3 Shadowgraph of a pellet

A shadowgraph gives an indication of a pellet size and shape. Photographs of a pellet are taken through a Polaroid camera by backlighting the pellet with a spark lamp (Xenon Corporation: model 437A Nanopulser) as shown in Fig. 7.

2.2.4 Ablation

A time evolution of the pellet ablation, e.g. the Balmer H_α or D_α line emission is measured in the horizontal direction by using a single photo-diode (Hamamatsu Photonics Corporation: S1226-5BQ) with an interference filter. The ablation profile as a function of the plasma radius can be obtained from this signal and the measured pellet velocity. Another diagnostic apparatus, which is 8 channel photo-diode array with a slit and an interference filter and viewes the pellet ablation in the vertical direction as shown in Fig. 8, can be obtained a local ablation and ablation profile from the envelope of peak intensity at each channel. Also, the velocity of the pellet travelling in a plasma can be evaluated from this measurement. The rise time of these detectors is about 2.8 μsec. Spatial resolution of this array is about 12 mm on the equatiorial plane.

2.2.5 Scattering of pellet trajectory

A Aℓ-foil target was installed 1.71 m downstream of the muzzule (Fig. 9). Scattering of trajectory for pellets from the gun barrel is monitored from scattering of holes on the Aℓ-foil.

3. Production and Injection of Pellet[10]

3.1 Condition of pellet production

Properties of hydrogen and deuterium gas below their critical temperature are shown in Table 1. When the temperature in the pellet carrier and main and barrel housings is less than 5-10°K, the hydrogen or deuterium gas easily freezes, and the solid pellet is produced. In the present pellet injection, the hydrogen gas freezes at about 5.6°K on the surface of the heat exchanger. The flow rate of liquid helium, which indicates the gas flow rate after evaporation of liquid helium, is about 100 ℓ/min. For deuterium pellet production, the flow rate of liq.He is 48-56 ℓ/min. and temperature is about 9.2°K. The flow rate of the fuel gas is 12-13 ℓ/min., and when the pressure near the production region of the pellet reaches at 400-430 Torr, a fuel supply is stopped. Cycle of pellet production and injection is about 3.5 minute.

The injector can be produced the mixed pellet of hydrogen and deuterium[14]. Production of the mixed pellet examined for three mixed gases with different ratio of hydrogen to the mixed gas (H_2+D_2). The ratio is about 39.8%, 23.5% and 6.3%, respectively. The temperature to freeze the mixed gas is about 7.2°K, and other condition is nearly the same with that of the hydrogen or deuterium pellet. The component of the mixed pellet is estimated from the component of mixed gas, which is measured by the mass spectrometer after the pellet is evaporated in the drift chamber. The component is different from that of the mixed gas before freezing as shown in Fig. 10. This may attribute to freezing temperature and gas pressure of supplied fuel. The detail control of temperature and pressure may be necessary to produce the mixed pellet with the desired component.

2.2.5 Scattering of pellet trajectory

A Aℓ-foil target was installed 1.71 m downstream of the muzzule (Fig. 9). Scattering of trajectory for pellets from the gun barrel is monitored from scattering of holes on the Aℓ-foil.

3. Production and Injection of Pellet[10]

3.1 Condition of pellet production

Properties of hydrogen and deuterium gas below their critical temperature are shown in Table 1. When the temperature in the pellet carrier and main and barrel housings is less than 5-10°K, the hydrogen or deuterium gas easily freezes, and the solid pellet is produced. In the present pellet injection, the hydrogen gas freezes at about 5.6°K on the surface of the heat exchanger. The flow rate of liquid helium, which indicates the gas flow rate after evaporation of liquid helium, is about 100 ℓ/min. For deuterium pellet production, the flow rate of liq.He is 48-56 ℓ/min. and temperature is about 9.2°K. The flow rate of the fuel gas is 12-13 ℓ/min., and when the pressure near the production region of the pellet reaches at 400-430 Torr, a fuel supply is stopped. Cycle of pellet production and injection is about 3.5 minute.

The injector can be produced the mixed pellet of hydrogen and deuterium[14]. Production of the mixed pellet examined for three mixed gases with different ratio of hydrogen to the mixed gas (H_2+D_2). The ratio is about 39.8%, 23.5% and 6.3%, respectively. The temperature to freeze the mixed gas is about 7.2°K, and other condition is nearly the same with that of the hydrogen or deuterium pellet. The component of the mixed pellet is estimated from the component of mixed gas, which is measured by the mass spectrometer after the pellet is evaporated in the drift chamber. The component is different from that of the mixed gas before freezing as shown in Fig. 10. This may attribute to freezing temperature and gas pressure of supplied fuel. The detail control of temperature and pressure may be necessary to produce the mixed pellet with the desired component.

3.2 Result of pellet injection test

3.2.1 Pellet velocity

The injection velocity of the pellet can be changed by setting the pressure of a propellant gas to different value. The gas is helium or hydrogen (the sound velocity is about 1000 m/s for helium and 1300 m/s for hydrogen at room temperature). Figure 11 shows the velocity as a function of propellant gas pressure. The pellet size is 1.65 mmϕ × 1.65 mmL in the pellet carrier disk. A solid line is a calculated velocity of a H_2-pellet on the basis of the ideal gun model given by Milors and Foster [15]. The propellant gas is helium at temperature of 288.16°K. The velocity (V_p) is given by the following equation.

$$P_o = \frac{2m_p C_o}{(\gamma+1)A_p}\frac{U_{max}}{L}\left[\frac{\gamma-1}{2}+\left(1-\frac{V_p}{U_{max}}\right)^{-(\gamma+1)/(\gamma-1)}-\frac{(\gamma+1)}{2}\left(1-\frac{V_p}{U_{max}}\right)^{-2/(\gamma-1)}\right] \quad \text{dyne/cm}^2$$

where P_o is pressure of the propellant gas, C_o is the sound velocity of propellant gas ($= \sqrt{\gamma RT/M}$), γ is specific heat of propellant gas, R is gas constant ($= 8.314 \times 10^7$ erg°K^{-1}mol^{-1}), T is temperature (°K) of propellant gas, M is molecular weight of propellant gas, m_p pellet mass, A_p is cross section of a gun barrel, L is length of a gun barrel, $U_{max} = 2C_o/(\gamma-1)$. Closed circles are experimental results of the H_2-pellet accelerated by He gas and crosses are the obtained velocity of the D_2-pellet propelled by H_2 gas. Data for the H_2-pellet indicate that velocities are 80 to 95% of the calculated velocity except some data at 10 kg/cm^2. In usual injection experiments, the velocity is 714-833 m/s. Reproducibility of the velocity is 80 to 90%. The maximum velocity for the D_2-pellet propelled by H_2 gas is about 970 m/s at 24 kg/cm^2.

3.2.2 Pellet mass

The D_2-pellet with the size of 1.65 mmϕ × 1.65 mmL includes deuterium atoms of about 2.15×10^{20} atoms. Under the good condition of freezing, the mass of the injected pellet is 71 to 90% of the maximum mass, corresponding to $1.5\text{-}1.9 \times 10^{20}$ atoms.

The microwave cavity is set in front of the gun barrel. It is

indicated from output of the detector (Fig. 6) that the mass-reproducibility of the pellet from the muzzle is very good. The data of pellet mass measured by two methods distribute from large to small values along the straight line going through origin in the diagram as shown in Fig. 12. These data indicate that small pellets produced in the carrier disk and injected from the muzzle. Sometimes, small pellets are injected into the drift chamber although the signal of the microwave cavity indicates large pellets. This may be due to the evaporation of the pellet during passing through the guide-tube.

3.2.3 Scattering of a pellet trajectory

An angular dispersion in a pellet trajectory in front of the entrance of JFT-2M is about 0.46° (the spread in the pellet trajectory is about 26 mm in diameter at a plasma center), as shown in Fig. 9.

3.2.4 Shadowgraph of an in-flight pellet

Figure 13 is a shadowgraph of an in-flight D_2-pellet with about 769 m/s. This indicates a pellet integrity. Some photographs show that pellets are broken or the edge of the pellet is lost.

3.2.5 Ablation of pellet

Figure 14(a) is the radial ablation profile of D_2-pellet obtained by using the 1 channel photo-diode with an interference filter. R_{out} is the distance from the major axis of the torus to the cross-point where the outside magnetic separatrix surface crosses the major radius in the equatorial plane. The pellet ablates just inside the magnetic separatrix surface in the auxiliary-heated discharge with single-null X-point. Ablation profiles are different by low confinement mode(L-mode) or high confinement mode(H-mode), divertor- or limiter-discharges, or electron temperature at a plasma boundary. Penetration depth depends on the size of pellet, pellet velocity and plasma parameters. Figure 14(b)-(e) indicates time histories of H_α/D_α line intensity (local ablation) at X = 0.0242, 0.0729, 0.1212 and 0.1725 m. X is a distance from a minor torus axis to the point where the midplane crosses a line of sight of the 8 channel photo-diode array. The envelope of the peak

intensity of local ablation at each channel against X indicates an ablation profile, which qualitatively agrees with the profile measured by using the horizontal photo-diode in Fig. 14(a). The pellet velocity in the plasma can be estimated from the plots of X versus times at peak intensity for each channel. This velocity agrees well with that obtained by the time of flight method on the injection line within the experimental uncertainty. The small hydrogen pellets (pellet size in the carrier = 1 mmϕ × 1 mmL) are injected in Ohmic heated plasmas with different electron density from 1×10^{19} to 3×10^{19} m^{-3}. Figure 15 shows the position of peak intensity of H_α line as a function of electron density. In the region of low density less than about 2×10^{19} m^{-3}, position of peak intensity decreases. This is due to the enhancement of ablation by run-away electrons, these electrons easily produced in the low density region. On the other hand, the position again decreases as the density increases. This tendency is reasonable according to the neutral shielding model of ablation by Milora and Faster[1]. The penetration depth of pellets (H_2, D_2) is measured in the auxiliary-heated plasmas with the limiter configuration. Figure 16 is the dependence of the penetration depth of pellets on the auxiliary-heated power (P_{NB} and P_{ICRF}). The electron density before pellet injection is $2.8\text{-}5.5 \times 10^{19}$ m^{-3} and pellet velocity is 714-769 m/s. The pellet size injected into discharges is estimated from the total intensity of H_α line, but the size in the carrier disk is 1.65 mmϕ × 1.65 mmL. The experimental results indicate that the penetration depth decreases as increasing of the heating power in both NB and ICRF heated discharges, but the depth in ICRF cases is larger than that in NB cases. In these experiments the ICRF heating is electron heating mode, so the number of the fast ions is small compared with that in NB cases. From the above-mentioned results, it is expected that the pellets can penetrate deeper even in higher ICRF power.

Figure 17 is the color photograph and tree-dimensional expression of D_2-pellet ablation in the NB($\sim$0.88 MW) heated deutrium plasma with single-null divertor configuration, which was taken by the flaming camera. The pellet life time is about 400 μs.

4. Experimental Results of Pellet Injection into Plasmas

Deuterium or hydrogen pellets are injected into an Ohmic heated plasmas and auxiliary-heated plasmas with limiter or divertor configuration. Ohmic heated discharges was sometimes disrupted by a single pellet injection, if the density rise was larger than 2×10^{19} m^{-3}.

4.1 Pellet injection in NB heated single-null divertor discharges

The single-null divertor discharges transfer from the lower confinement mode (L-mode) to the high confinement mode (H-mode) during auxiliary heating. The global energy confinement time (τ_E) recovers up to that in Ohmic heating[16]. Pellets were injected into the L-mode or H-mode in order to improve the plasma properties [12]. The global energy confinement time is calculated according to the energy balance equation, that is the definition of confinement time (τ_E) is as follows,

$$\tau_E = W_s/(P_{total} - dW_s/dt) \ ,$$

where W_s is plasma stored energy, P_{total} is total input power.

In the first injection experiments, the deuterium pellet was fueled before H-transition (in L-mode). The injection velocity is about 700 m/s. The hydrogen NB of 34 keV was injected into the deuterium plasmas with upper single-null divertor configuration at 650 ms, heating power injected from the port is about 0.77 MW (net heating power by the calculation of NB power deposition code is about 0.67 MW). The magnetic configuration in the series experiments is shown in Fig. 18. The outer magnetic surface, which is closed surface of about 5 mm inner from the separatrix surface, null point and some configuration parameters determined by the magnetic fitting method. Three different types of discharges with pellet fueling are classified under these conditions.

The increment of $\bar{n}_e$ at the pellet injection time ($\Delta\bar{n}_e$ measured by the HCN laser interferometer) is about 1.5×10^{19} m^{-3} as shown in Fig. 19. Subsequently, the density is increasing linearly with time. The D_α line intensity near the limiter or the location of the gas puffing decreases after the pellet injection. These time behaviors of $\bar{n}_e$ and D_α line indicates that the particle recycling reduced and the particle confinement

was improved. The radiation loss power including the charge exchanged particle loss is increasing linearly up to the time of sudden increase of D_α line intensity. The global energy confinement time is determined from the magnetic fitting method assuming the constant internal inductance. After pellet injection, τ_E is nearly the same value as that of ohmically heated discharges at the same density region, but decreases gradually as increasing the density and the radiation loss power. This degradation may be due to the increase of the radiation loss power from the central region of the plasma. These properties are similar to that in the H-mode achieved in the gas fueled discharges.

The second discharges are the very high confinement mode (pellets are fueled in the L-mode). $\Delta\bar{n}_e$ is about 4.5×10^{19} m^{-3}. The ablation profile of this large pellet was horizontally measured by the single H_α/D_α detector. A local ablation rate at the point of X = 0.1725 m, X = 0.1212 m, X = 0.0729 m and X = 0.0242 m can be also estimated from the signals in Fig. 20. These signals show that the pellet is ablating mainly around r = 0.1 m (R = 1.4 m) and passing through the center of the plasma column. W_S is linearly increasing and when W_S reaches 34 kJ, $\dot{\tilde{B}}_\theta$ signal always grows and the plasma energy is bursted out (Fig. 21). The frequency of the $\dot{\tilde{B}}_\theta$ is about 5 kHz, and the $\dot{\tilde{B}}_\theta$ signal grows at the safety factor (q_ψ) of the outer magnetic surface close to 2.5. As this time, $<\beta_t>$ is about 1.6%, and the factor of g according to the equation of $<\beta_t> = gI_p/(aB_t)$ [17] is about 2.2. This results agree with the range of theoretical limits due to kink and ideal ballooning modes with free boundary. The burst-out of plasma energy is considered to be caused by the β-limit. During increasing of W_S, about of 70% of net NB heated power is stored in the plasma (dW_S/dt is shown in Fig. 21). The increment of W_S is mainly due to the increase of both electron and ion temperatures (T_e^{SX}, T_i^{CX}), which are obtained by the soft X-ray energy spectra analysis and mass separated neutral particle energy spectra analysis, respectively. Both electrons and ions are cooled down, following the pellet injection, but after about 30-40 ms both electron and ion temperatures are approximately the same and the plasmas heat to about 0.8 keV as shown in Fig. 22. The radiation loss and D_α line intensity do not increase up to the time of the saturation of W_S. These facts indicate that impurity accumulation into a plasma core and particle recycling rate is very little in this case compared with that in the H-mode. τ_E increases to 60-75 ms and this level is sustained

for about 20 ms. The value exceeds that in Ohmically heated discharges by a factor of 1.4-1.7. However, the duration sustained very high confinement is shorter than τ_E, so the discharges is transient. This is due to the growth of MHD oscillation with large amplitude.

In the another discharges with properties of very high confinement (τ_E = 60-75 ms) by pellet injection with $\Delta\bar{n}_e = 4 \times 10^{19}$ m^{-3} (Fig. 23), W_s saturates, P_R increases and τ_E degrades to about 35 ms (near the H-mode level) following $\dot{\tilde{B}}_\theta$ signal growing (P_R keeps lower level during very high confinement phase). The ablation profile is similar to that in the above-mentioned case (Fig. 24). The characteristics of this discharges are concluded that the very high confinement mode terminates when $<\beta_t>$ taches close to the β-limit softly, and the discharges turns to the H-mode.

Figure 25 shows the global energy confinement time as a function of the line averaged electron density. τ_E in the Ohmic heating increases linearly with $\bar{n}_e$ up to $\bar{n}_e = 4 \times 10^{19}$ m^{-3} and saturates at about 50 ms. τ_E in the small pellet fueled discharges is 50-55 ms and degrades to the level of H-mode in the gas-fueled discharges. The very high confinement (60-75 ms) achieved around $\bar{n}_e$ of 6×10^{19} m^{-3} by the large pellet.

In the second injection experiments, pellets were fueled in the H-mode discharges during NB heating. The pellets much ablate near the peripheral region (more outside than in the L-mode injection cases) as shown in Fig. 26. This is due to enhancement of ablation by the fast ions, which are produced through the charge exchange process between NB and plasma ions. The plasma in the peripheral region is strongly cooled. So, the stored energy dropps rapidly following radiation loss increase (Fig. 27). W_s does not recover to the level without pellet injection. The global energy confinement time deteriorates. The degree of the degradation of W_s becomes smaller as the injection timing is earlier.

4.2 Pellet injection in the ICRF heated single-null divertor discharges[12]

In ICRF heated discharges with the lower single-null configuration (Fig. 28), the plasmas are transferred to the H-mode as well as in the NB heated discharges. The large deuterium pellet ($\Delta\bar{n}_e$ = 3-4 $\times 10^{19}$ m^{-3}) was injected into the L-mode divertor discharges with the number-density

ratio of hydrogen to deuterium (n_H/n_D) of about 30%. The ICRF launched power P_{rf} is 0.6-0.8 MW (from 600 to 900 ms).

Figure 29 shows the behaviors of $\bar{n}_e$, W_s, $\dot{B}_\theta$, $\dot{W}_s$, $I^{D\alpha}$ (solid line: in divertor region, dotted line: in main plasma region), and P_R, which are very similar to those in the discharges heated by NB (see §4.1) except the behavior after about 760 ms. In this type discharge, the plasma stored energy continuously increases, and the global energy confinement time (τ_E) rises up to 55-60 ms, keeping this level for about 20 ms (transient phenomena), and P_R sharply increases following a subsequent decrease untill large MHD oscillation grows. According to the MHD oscillation growing, the radiation loss power again increases and confinement time decreases although the electron density is continuously increasing. This is due to accumulation of an impurity into a plasma center as spectroscopic measurements of iron line emissions (FeX, FeXVIII) indicate. After MHD oscillation growing, impurity looks like to repeat accumulation and exhaust.

Sometimes, discharges characterized by transiently very-high confinement are disrupted at about 40 ms after pellet injection, which comes from rapid and large growth of MHD oscillation and rapid increase of radiation loss power as shown in Fig. 30. Then, maximum W_s is about 32 kJ, and volume averaged toroidal beta value $<\beta_t>$ is about 1.3%, corresponding to Toroyan factor $g = 1.6$. Thus, the plasma disruption attributes to a large amount of radiation cooling and is not due to beta limit. Figure 31 shows the ablation profile obtained from the horizontal measurement of D_α line emission. R_{out} is a major radius crossed an outside separatrix surface in the midplane and R is the local position of the plasma from the major axis of the torus. The pellet penetrated deeply in a core plasma, exceeding a minor axis of a torus ($R = 1.31$ m) as drawn by a solid line. Maximum ablation is around $R_{out} - R = 1.2$ m e.g., about one half of the plasma minor radius. The dotted line indicates a profile of the pellet ablation in L-mode during NB heating.

The second discharges with the deuterium pellet injection in the H-mode have the electron density rise of about 3×10^{19} m^{-3} (Fig. 32). Radiation loss after pellet fueling is slightly large compared with that in the discharges fueled the pellet in the L-mode. W_s continuously increases up to about 35 kJ until the radiation begins to increase. These characteristics are significantly different from that for injection

in H-mode during NB heating. Energy confinement time is improved up to about 50 ms around $\bar{n}_e = 6 \times 10^{19}$ m^{-3}. This value exceeds τ_E in Ohmic heating as shown in Fig. 33. Electron temperature T_e^{SX}, which is obtained from analysis of soft X-ray spectrum measured in the tangential direction, decreases immediately after the injection from approximately 1.35 keV to less than 1.1 keV, immediately following the injection and recovered up to the value before pellet injection (Fig. 34). The pellet ablation profile is shown in Fig. 31 by a broken line. The pellet is ablated slightly more outside than in L-mode cases in ICRF or NB heatings. Most of the pellet is ablated around $R_{out} - R = 0.15$ m. Ablation in a scrape-off layer is very little as in other cases. In NB heated discharges with the pellet injection in the H-mode, the pellet is strongly ablated just inside separatrix layer compared with above-mentioned cases.

The global energy confinement time (τ_E) linealy improved with $\bar{n}_e$ in the range of 4-6.2 $\times 10^{19}$ m^{-3}on $\bar{n}_e - \tau_E$ diagram as shown in Fig. 33. The maximum confinement time in both H-mode and L-mode is about 1.4-1.7 times as large as that in Ohmic heating around $\bar{n}_e = 6 \times 10^{19}$ m^{-3}. On the other hand, the confinement time for the H-mode without pellet in ICRF heated single-null divertor discharges is 30-40 ms for 4-6 $\times 10^{19}$ m^{-3} and P_{total} = 0.8-1.1 MW, which is in comparison with τ_E in Ohmic heating. Above-mentioned experimental results reveal that the energy confinement time can be improved by pellet fueling in L-mode and H-mode during ICRF heating on the single-null X-point operation, although the phenomena are transient.

4.3 Pellet injection in the NB+ICRF heated limiter discharges

The deuterium pellet is injected in the D-shaped limiter discharges (deuterium plasmas) with auxiliary heating combined NB and ICRF. The power of NB is about 0.8 MW and the launched power of ICRF is about 1.8 MW. Figure 35 is the magnetic configuration. The plasma current at the flat top is about 381 kA, B_t is 1.19 T, the ellipticity (κ) is about 1.55 and q_ψ is 3.54 at 750 ms. The plasma is contact with the inner fixed limiter and is separated from outer fixed limiter. The deuterium pellet is injected in the saturation phase of W_s and P_R during ICRF heating and just before NB start (before about 10 ms). After pellet injection, W_s linearly increased up to about 80 kJ, this value is maximum

in the JFT-2M discharges as shown in Fig. 36. The key point to obtaine this discharge is adjustment of timing of pellet injection. The electron temperature measured by soft X-ray spectrum analyser is recovered up to about 1.5 keV (Fig. 37). Figure 38 shows the ablation profile of the pellet with the injected velocity of about 769 m/s. The pellet reached inner side, exceeding the minor axis of the torus. The maximum deposition of the particle is near the major axis R = 1.31 m, corresponding to about one half of the minor radius of the plasma. The electron density is missed in the discharges.

5. Summary and Future Plan

The single-pellet injection experiments and the pellet injector developed for JFT-2M were reviewed. These studies and development of the injector are summarized as follows.

Injection Experiments

(1) The global energy confinement time can be improved by pellet injection in the L-mode of NB and ICRF heatings and in the H-mode of ICRF heating.

τ_E = 60-75 ms for NB heated L-mode plasmas

τ_E = 55-60 ms for ICRF heated L-mode plasmas

τ_E = 50 ms for ICRF heated H-mode plasmas

(2) The particle confinement time can be improved by pellet injection, ---- particle recycling does not increase ($\bar{n}_e$ increases and maintaines higher level, and increase of H_α/D_α line emission is little).

(3) Electron and ion temperatures go up to initial level or higher level before pellet injection for 30-40 ms, although temperatures suddenly decrease at pellet injection.

(4) Radiation loss power, including charge exchanged particle loss is not large during maintaining improved confinement, ---- supply of pure fuel is possible and impurity accumulation into a central region of the plasma is suppressed by pellet injection.

(5) Plasma stored energy can be increased by optimization of injection timing of pellet and auxiliary heating (NB, ICRF).

It was found from these results that the pellet fueling in the

in the JFT-2M discharges as shown in Fig. 36. The key point to obtaine this discharge is adjustment of timing of pellet injection. The electron temperature measured by soft X-ray spectrum analyser is recovered up to about 1.5 keV (Fig. 37). Figure 38 shows the ablation profile of the pellet with the injected velocity of about 769 m/s. The pellet reached inner side, exceeding the minor axis of the torus. The maximum deposition of the particle is near the major axis R = 1.31 m, corresponding to about one half of the minor radius of the plasma. The electron density is missed in the discharges.

5. Summary and Future Plan

The single-pellet injection experiments and the pellet injector developed for JFT-2M were reviewed. These studies and development of the injector are summarized as follows.

Injection Experiments

(1) The global energy confinement time can be improved by pellet injection in the L-mode of NB and ICRF heatings and in the H-mode of ICRF heating.

τ_E = 60-75 ms for NB heated L-mode plasmas

τ_E = 55-60 ms for ICRF heated L-mode plasmas

τ_E = 50 ms for ICRF heated H-mode plasmas

(2) The particle confinement time can be improved by pellet injection, ---- particle recycling does not increase ($\bar{n}_e$ increases and maintaines higher level, and increase of H_α/D_α line emission is little).

(3) Electron and ion temperatures go up to initial level or higher level before pellet injection for 30-40 ms, although temperatures suddenly decrease at pellet injection.

(4) Radiation loss power, including charge exchanged particle loss is not large during maintaining improved confinement, ---- supply of pure fuel is possible and impurity accumulation into a central region of the plasma is suppressed by pellet injection.

(5) Plasma stored energy can be increased by optimization of injection timing of pellet and auxiliary heating (NB, ICRF).

It was found from these results that the pellet fueling in the

plasmas was effective to improve plasma properties.

Development of Injector

The single pneumatic-gun type injector was developed.

(1) Pellet velocity is 970 m/s at maximum and 714-833 m/s in usual injection experiments. These velocities correspond to 80-95% of the velocity calculated from the ideal gun model.

(2) Pellet mass is 71-90% of the designed pellet mass.

(3) Hydrogen, deuterium and mixed (H_2+D_2) gas can be frozen for solid pellet.

(4) Microwave cavity method to measured the pellet mass was developed and 8 channel H_α/D_α photo-diode array with fast response was constructed to measure the ablation profile and the pellet velocity in the plasmas.

Lastly, the future plan of the pellet injection experiments and development of the pellet injector are shown in Fig. 39. In JFT-2M, the injection experiments with 4 pellet injector have been started from April in 1987. An optimization of refueling cycle, impurity transport, improvement of τ_E, heating efficiency and high density (density limit), and density profile control during auxiliary heating are investigating.

In the next step, the technical development to make multi-pellet and to obtain high velocity more than 2 km/s is very important in fueling experiments. Three steps of development are proposed, e.g. development of high velocity (2-2.5 km/s) multi-pellet injector, of very high speed (2.5-5 km/s) pellet (single or multi) injector and of hypervelocity pellet injector. These injectors will be tested performance and installed the large machine (JT-60, FER) with long pulse and high-power heated plasmas to study refueling, improvement of plasma confinement, impurity control and density profile control. And the tritium pellet injection system should be developed for FER or a reactor in future, in parallel with the above-mentioned steps as shown in Fig. 39.

Acknowledgements

The authors would like to acknowledge Drs. A. Funahashi and Y. Tanaka for their encouragements and support of this work. They are also indebted to the members in Experimental Plasma Physics Laboratory for their useful discussion, to Messers. K. Suzuki, Y. Matsuzaki, T. Tani, T. Shibata and other members in Facility Operation and Engineering Division for their operation of JFT-2M, neutral beam heating device and pellet injector and Dr. H. Ohtsuka for his taking the photograph of pellet ablation. They gratefully acknowledge Drs. M. Tanaka, K. Tomabechi and S. Mori for their continuous encouragements.

References

[1] MILORA, S.L., J. Fusion Energy 1 (1981) 15, MILORA, S.L., FOSTER, C.A., THOMAS, C.E., BUSH, C.E., WILGEN, J.B., et al., Nucl. Fusion 20 (1980) 1491.

[2] GREENWALD, M., PARKER, J., BESEN, M., FIORE, C.L., FOOD, M., et al., in Controlled Fusion and Plasma Physics (Proc. 11th Europ. Conf., Aachen, 1983), Vol.7D, Part I, European Physical Society (1983) 7.

[3] EQUIPE TFR, in Plasma Physics and Controlled Nuclear Fusion Research 1984 (Proc. 10th Int. Conf., London, 1984), Vol.1, IAEA, Vinna (1985) 103.

[4] MILORA, S.L., SCHMIT, G.L., HOULBERG, W.A., ARUNASALAM, V., ATTENBERGER, S.E., et al., Nucl. Fusion 22 (1982) 1263.

[5] HOSEA, J., BELL, R., BITTER, M., CAVALLO, A., COHEN, S., et al., in Controlled Fusion and Plasma Physics (Proc. 12th Europ. Conf., Budapest, 1985), Vol.9F, Part II, European Physical Society (1985) 120.

[6] VLASES, G., BUCHL, K., CAMPBELL, D., in Controlled Fusion and Plasma Physics (Proc. 11th Europ. Conf., Aachen, 1983), Vol.7D, Part I, European Physical Society (1983) 127.

[7] SENGOKU, S., ABE, M., HOSHINO, K., ITOH, K., KAMEARI, A., et al., in Plasma Physics and Controlled Nuclear Fusion Research 1984 (Proc. 10th Int. Conf., London, 1984), Vol.1, IAEA, Vinna (1985) 405.

[8] HAWRYLUK, R.J., ARUNASALAM, V., BELL, M.G., BITTER, M., BLANCHARD, W.R., et al., 11th Int. Conf. on Plasma Physics and Controlled Nuclear Fusion Research, IAEA-CN-47/A-I-3, Kyoto (1986), SCHMIT, G.L., MILORA, S.L., BELL, M.G., BITTER, M., BUSH, C.E., et al., in Controlled Fusion and Plasma Physics (Proc. 12th Europ. Conf., Budapest, 1985), Vol.9F, Part II, European Physical Society (1985) 674.

[9] GONDHALEKER, A., CHEETHAM, A., BURES, M., CAMPBELL, D., COHEN, S.A., et al., 11th Int. Conf. on Plasma Physics and Controlled Nuclear Fusion Research, IAEA-I-1-6, Kyoto (1986).

[10] KASAI, S., MIURA, Y., HASEGAWA, K., SENGOKU, S., OGAWA, H., et al., Japan Atomic Energy Research Institute Report, JAERI-M 86-109 (1986), "First Results of Pellet Injection Experiments in JFT-2M Additionally Heated Plasmas", KASAI, S., HASEGAWA, K., MIURA, Y., ISHIBORI, I., Japan Atomic Energy Research Institute Report, JAERI-M 86-035 (1986), "Production and Ejection of Solid Hydrogen-Isotope Pellet (Single Pellet)", (in Japanese).

[11] Mitsubishi Atomic Power Industries Inc., Report of Consignation Study in PY.1982 (1983), "Development of High Speed Pellet Injector for Fueling", (in Japanese).

[12] KASAI, S., MIURA, Y., SENGOKU, S., HASEGAWA, K., Int. Pellet Fueling Workshop, San Diego (1985), "JFT-2M Pellet Injection Experimental Results", MIURA, Y., KASAI, S., SENGOKU, S., HASEGAWA, K., SUZUKI, N., et al., Japan Atomic Energy Research Institute Report, JAERI-M 86-148 (1986), "Characteristics of Pellet and Neutral Beam Injected Single Null Divertor Discharges of the JFT-2M Tokamak", KASAI, S., MIURA, Y., SENGOKU, S., HASEGAWA, K., OGAWA, H., et al., Japan Atomic Energy Research Institute Report JAERI-M 87-159 (1987), "Improvement of Confinement in Auxiliary Heated (ICRF) Divertor Discharges by Pellet Injection".

[13] SENGOKU, S., KASAI, S., MIURA, Y., HASEGAWA, K., Read at Autumn Meeting of Phys. Soc. of Jpn., Kobe, September 1986, Vol.4, 27PM-10, P176, JENSEN, P.B., ANDERSEN, V., J. Phys. D : Appl. Phys. 15 (1982) 785.

[14] HASEGAWA, K., KASAI, S., MIURA, Y., ISHIBORI, I., Japan Atomic Energy Research Institute Report JAERI-M 87-162 (1987), "Production and Injection of Hydrogen-Deuterium Mixed Pellet", (in Japanese).

[15] MILORA, S.L., FOSTER, C.A., Rev. Sci. Instrum 50 (1979) 482, MILORA, S.L., J. Fusion Energy 1 (1981) 15.

[16] SENGOKU, S. and JFT-2M team, 7th Int. Conf. on Plasma Surface Interaction, Princeton (1986), ODAJIMA, K., FUNAHASHI, A., HOSHINO, K., KASAI, S., KAWAKAMI, T., et al., 11th Int. Conf. on Plasma Physics and Controlled Nuclear Fusion Research, IAEA-CN-47/A-III-2, Kyoto (1986).

[17] TOROYON, F., GRUBER, R., SAURENMANN, H., SEMENZATO, S., SUCCI, S., Plasma Physics and Controlled Fusion 26 (1984) 209.

Table 1 Properties of hydrogen and deuterium gas below critical temperature

	H_2	D_2
(1) Mass Density (g/cm^3) (Solid at T= 4.2°K)	8.93×10^{-2}	2.04×10^{-1}
(2) Triple Point		
T (°K)	13.8	18.7
P (Torr)	53	169
(3) Sublimation Energy (cal/g) (at 4.2°K)	97.22	71.06

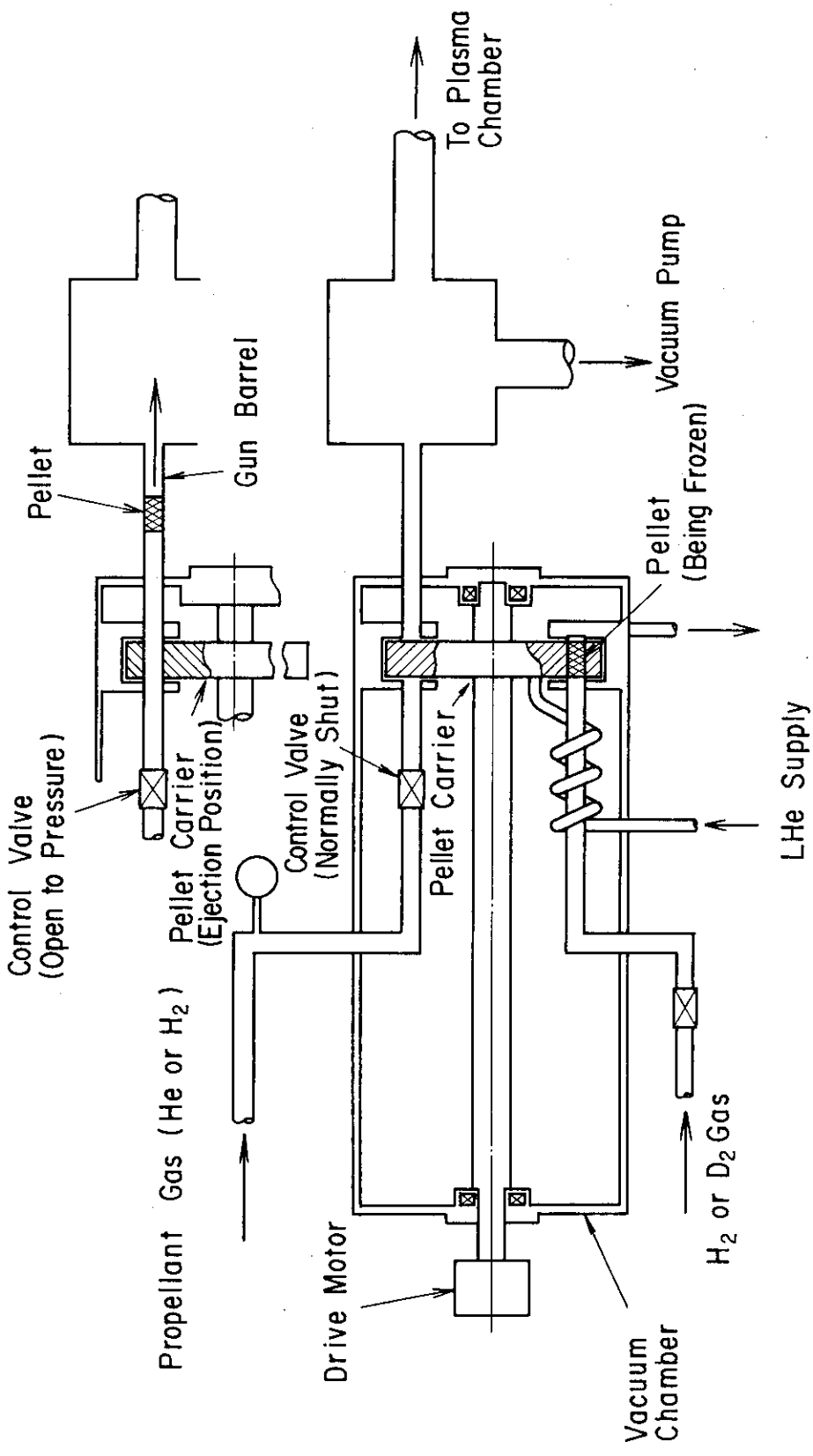

Fig. 1 Principle of pellet injector, H_2 or D_2 gas is freezed by liquid He and the pellet is accelerated by pressurized gas (H_2, He).

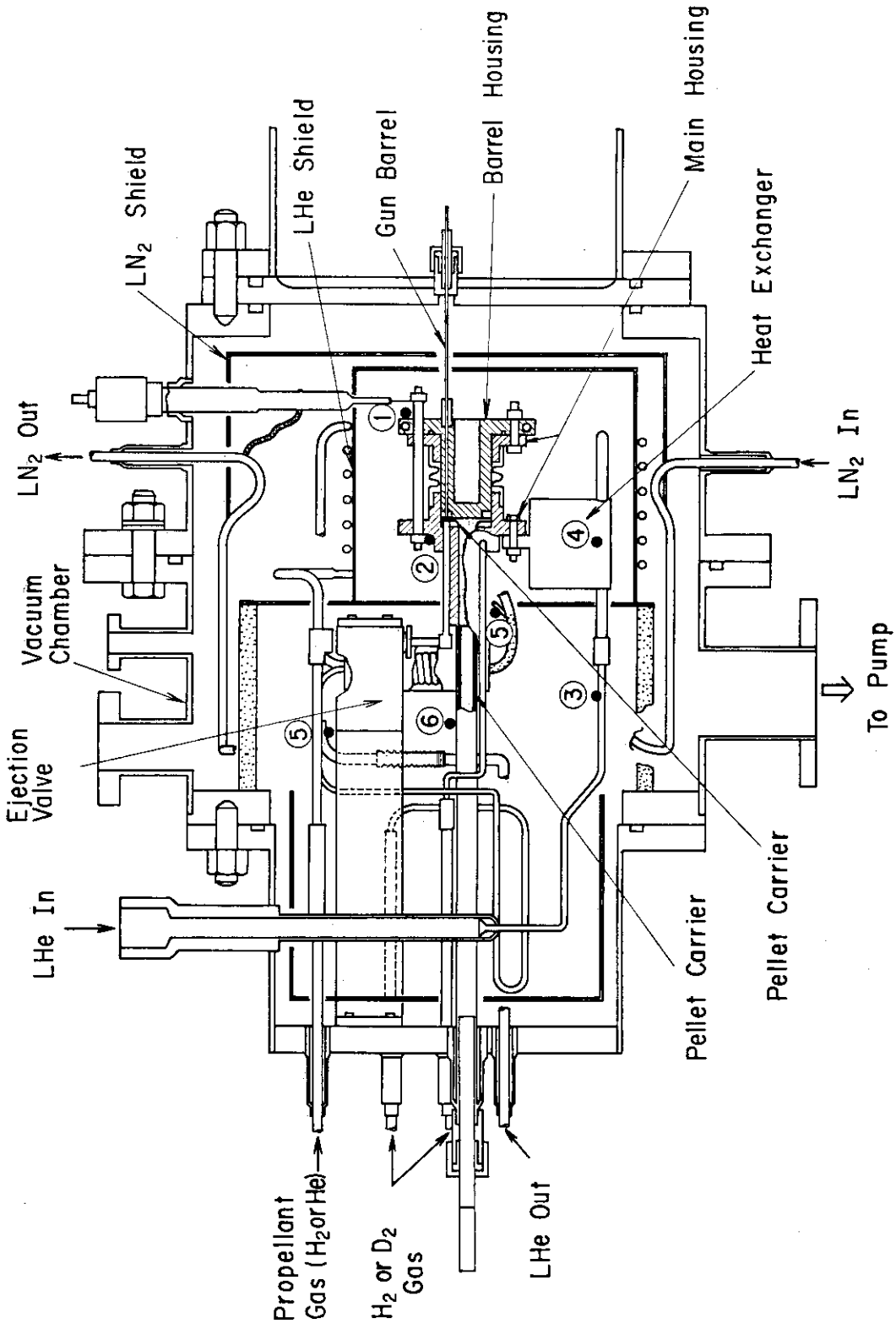

Fig. 2 Pneumatic single-pellet injector for JFT-2M.

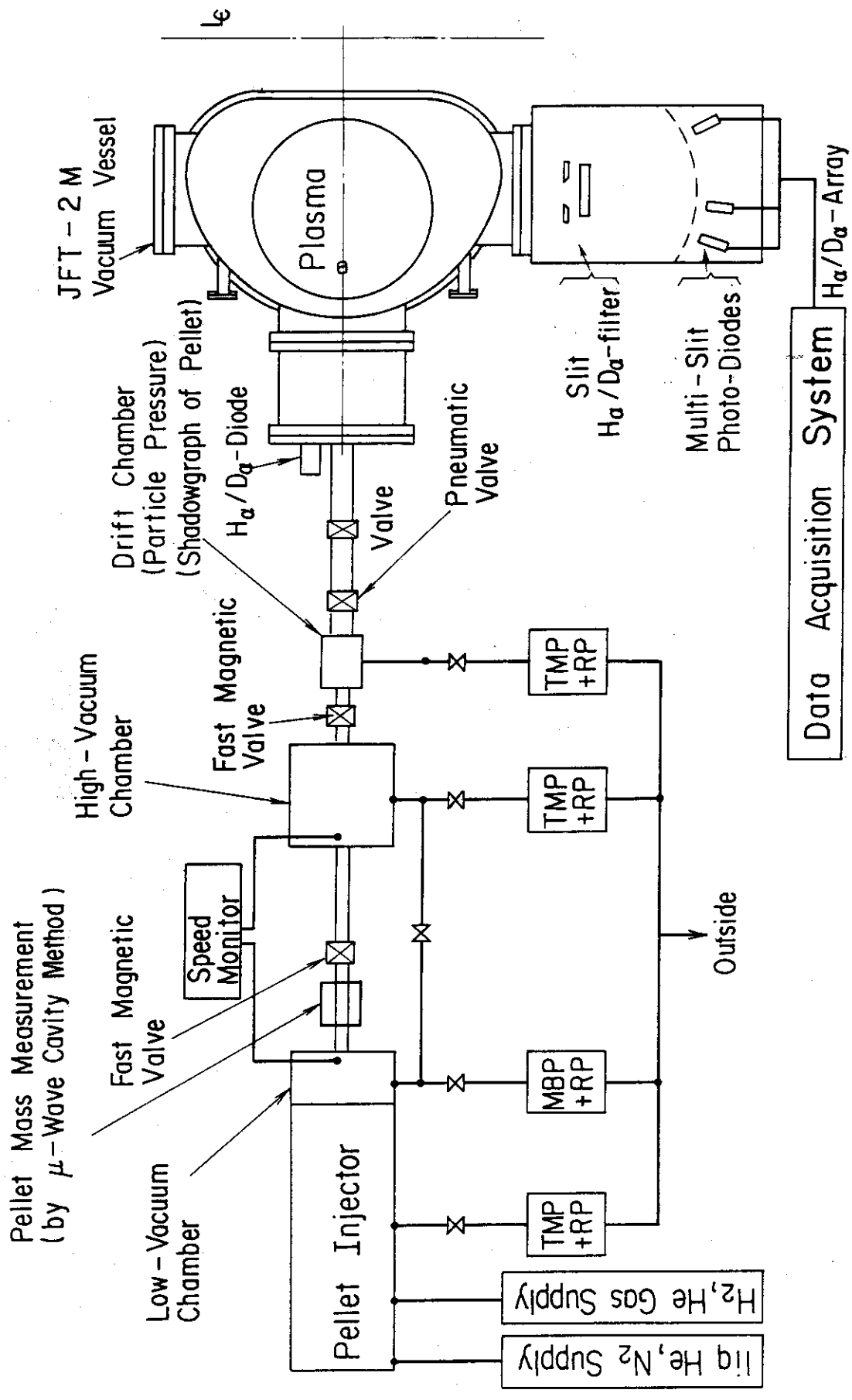

Fig. 3 Schematic diagram of the single-pellet injector and injection line for JFT-2M.

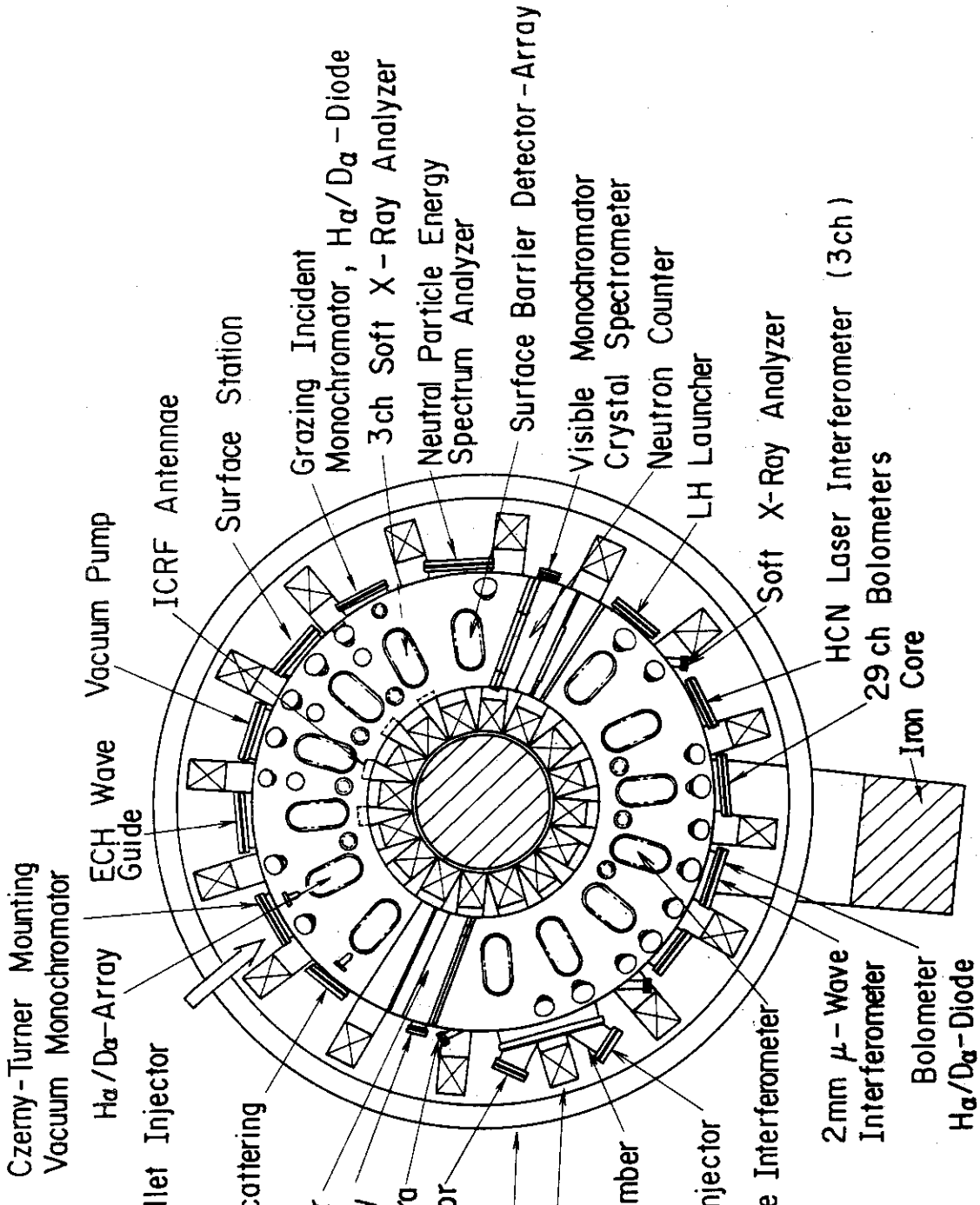

Fig. 4 Plane view of JFT-2M, and arrangement of the pellet injector, auxiliary heating system and plasma diagnostic apparatuses.

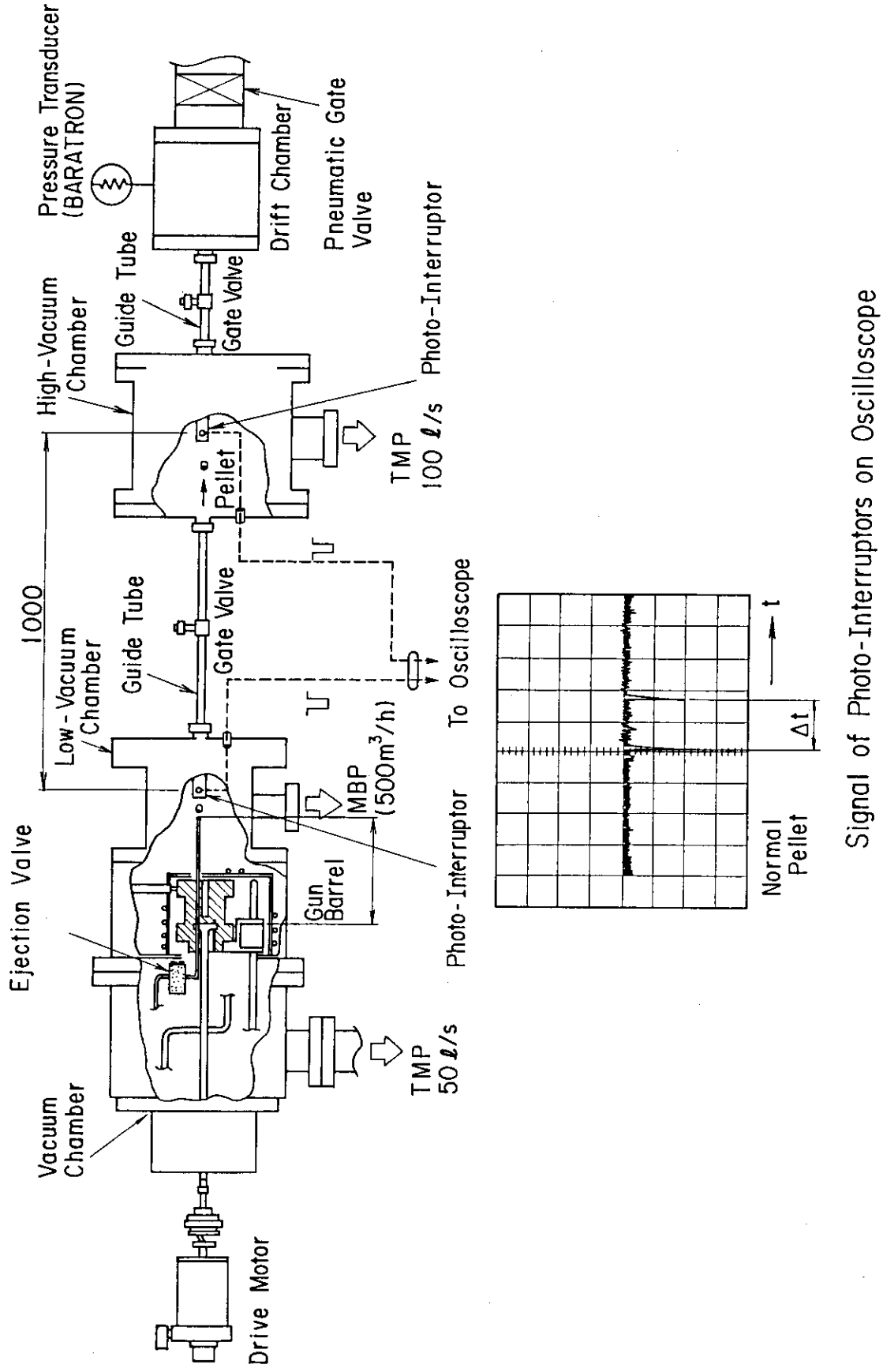

Fig. 5 System of pellet velocity measurement.

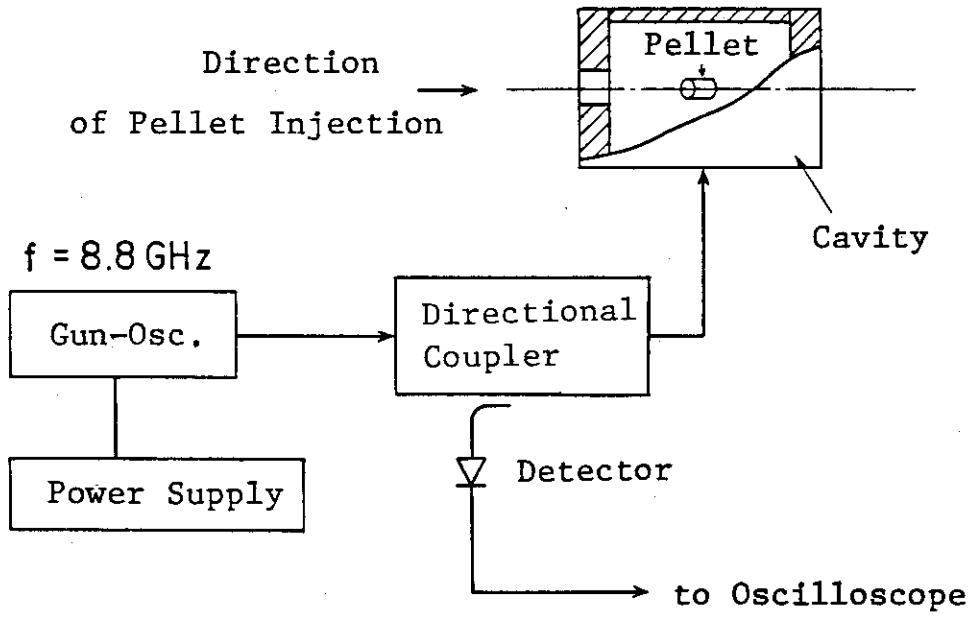

Fig. 6 Block diagram of pellet mass measurement by microwave cavity method.

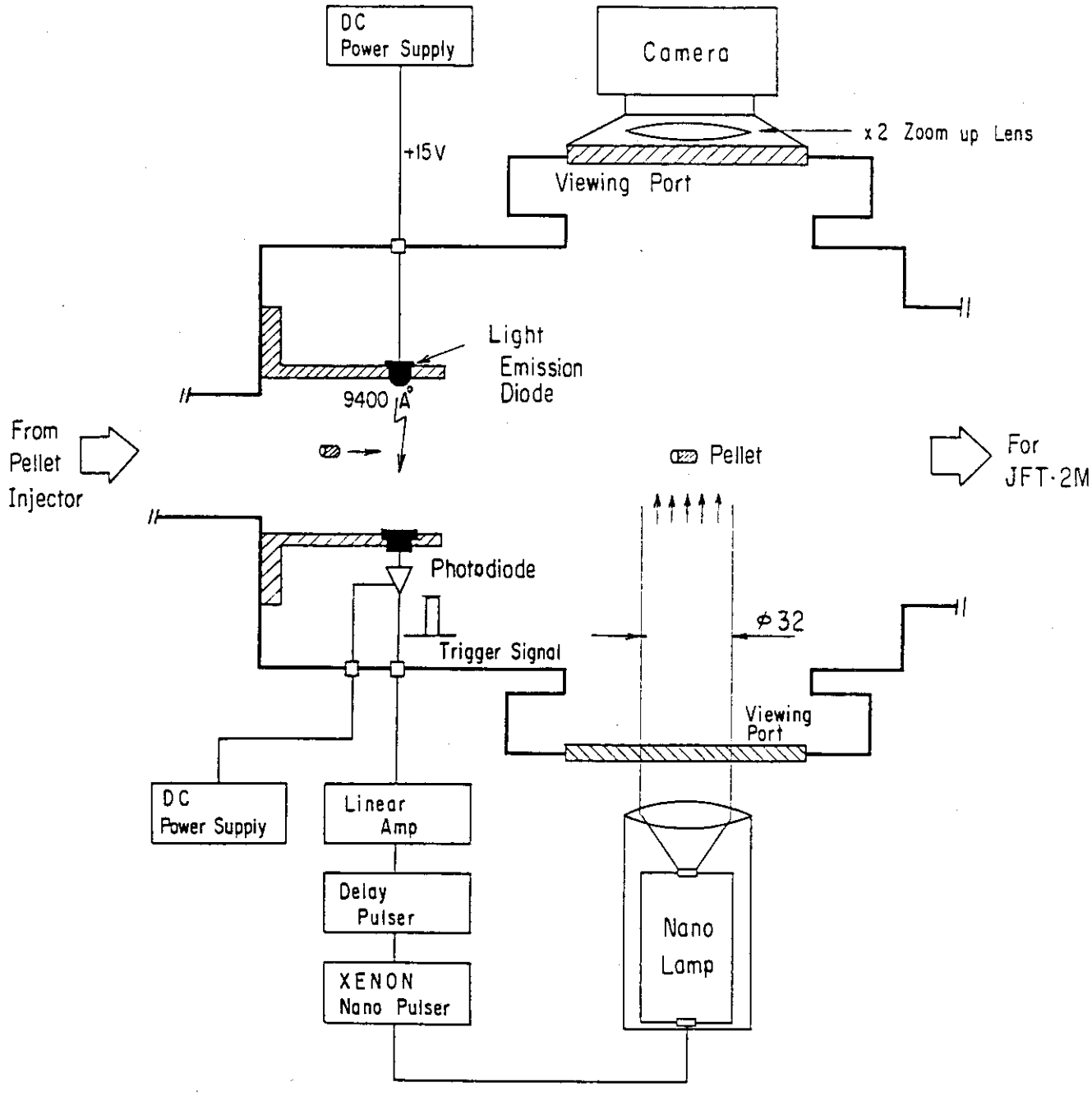

Fig. 7 System of pellet-shadowgraph measurement.

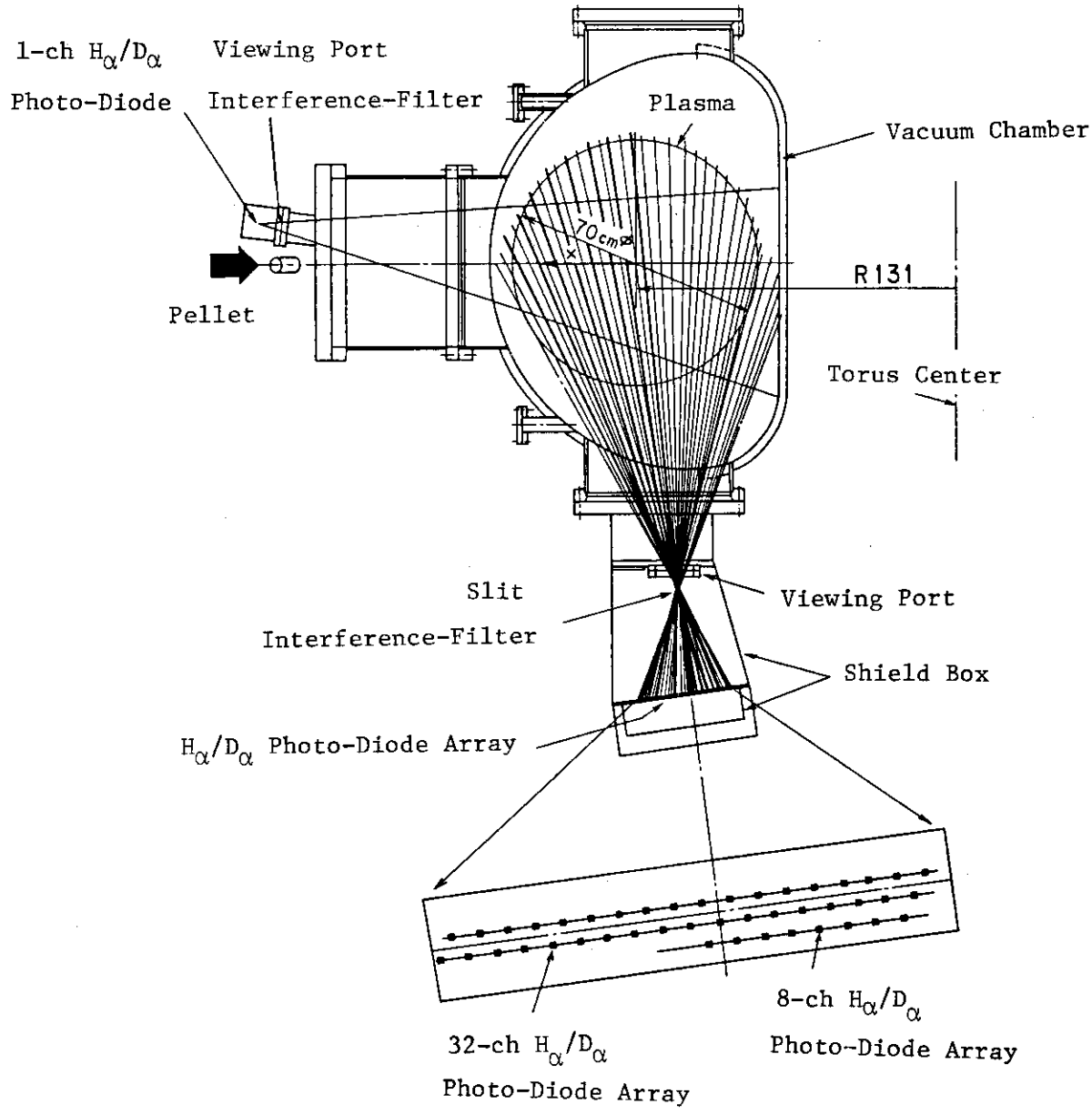

Fig. 8 System of pellet ablation measurement.

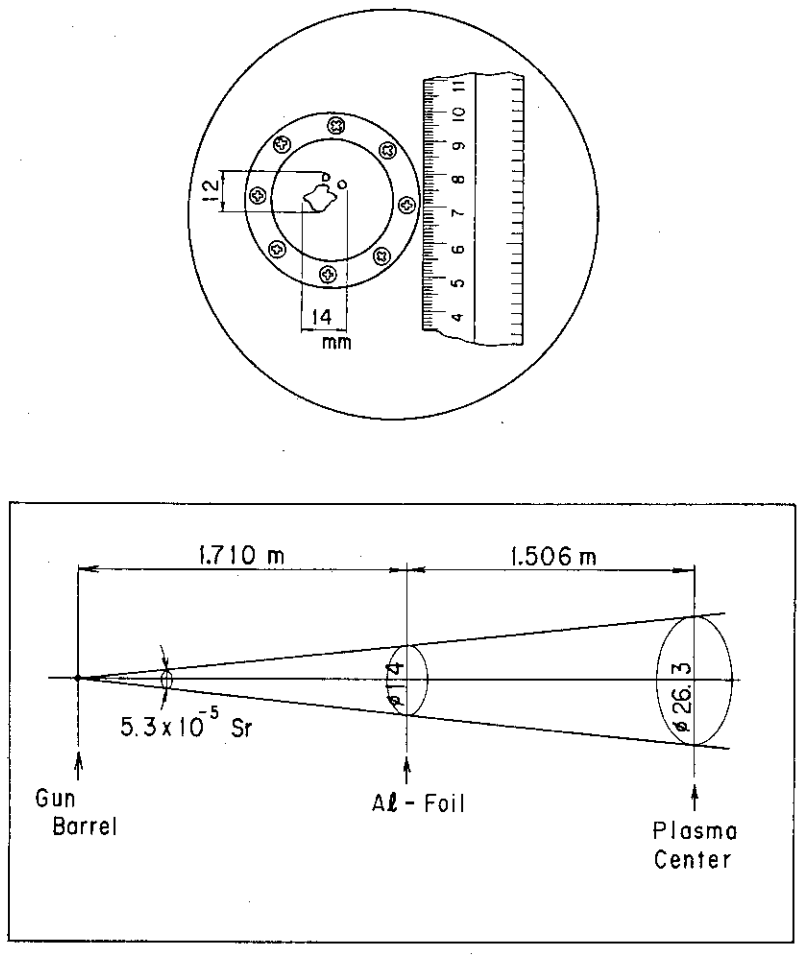

Fig. 9 Measurement of scattering of pellet trajectory.

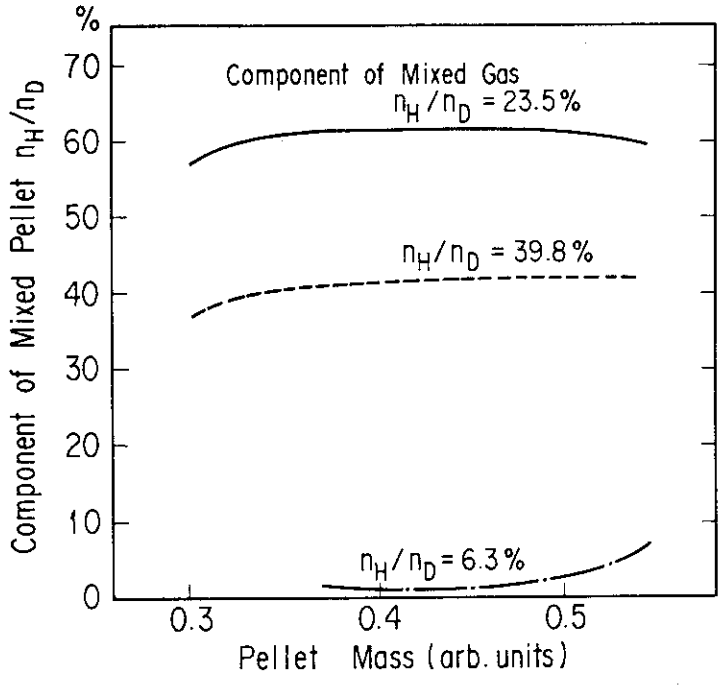

Fig. 10 Component of mixed pellet (H_2+D_2), n_H/n_D versus pellet mass

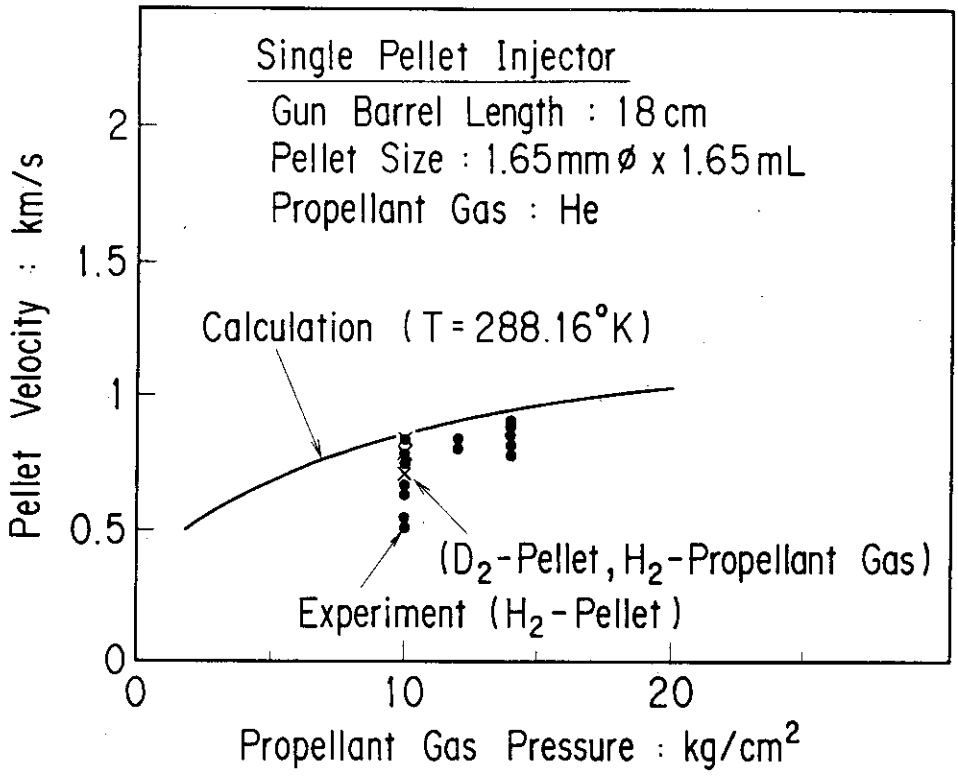

Fig. 11 Dependence of pellet velocity on propellant gas pressure. Closed circles are measured velocity of H_2-pellet (propellant gas is He) and crosses are measured velocity of D_2-pellet (propellant gas is H_2). Solid line is calculated velocity of H_2-pellet accelerated by He gas.

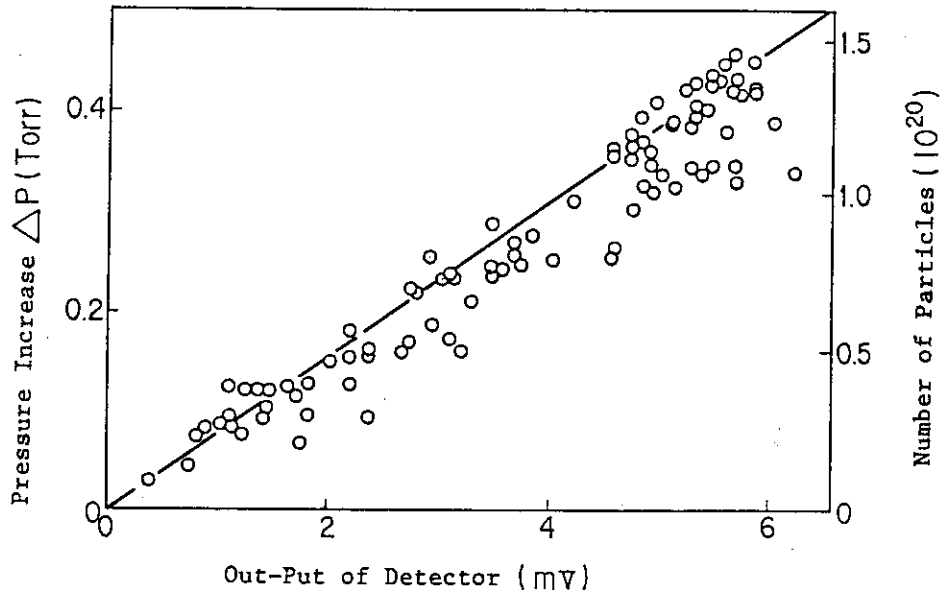

Fig. 12 Pressure rise by evaporation of pellet in the drift chamber versus output of detector in microwave cavity method.

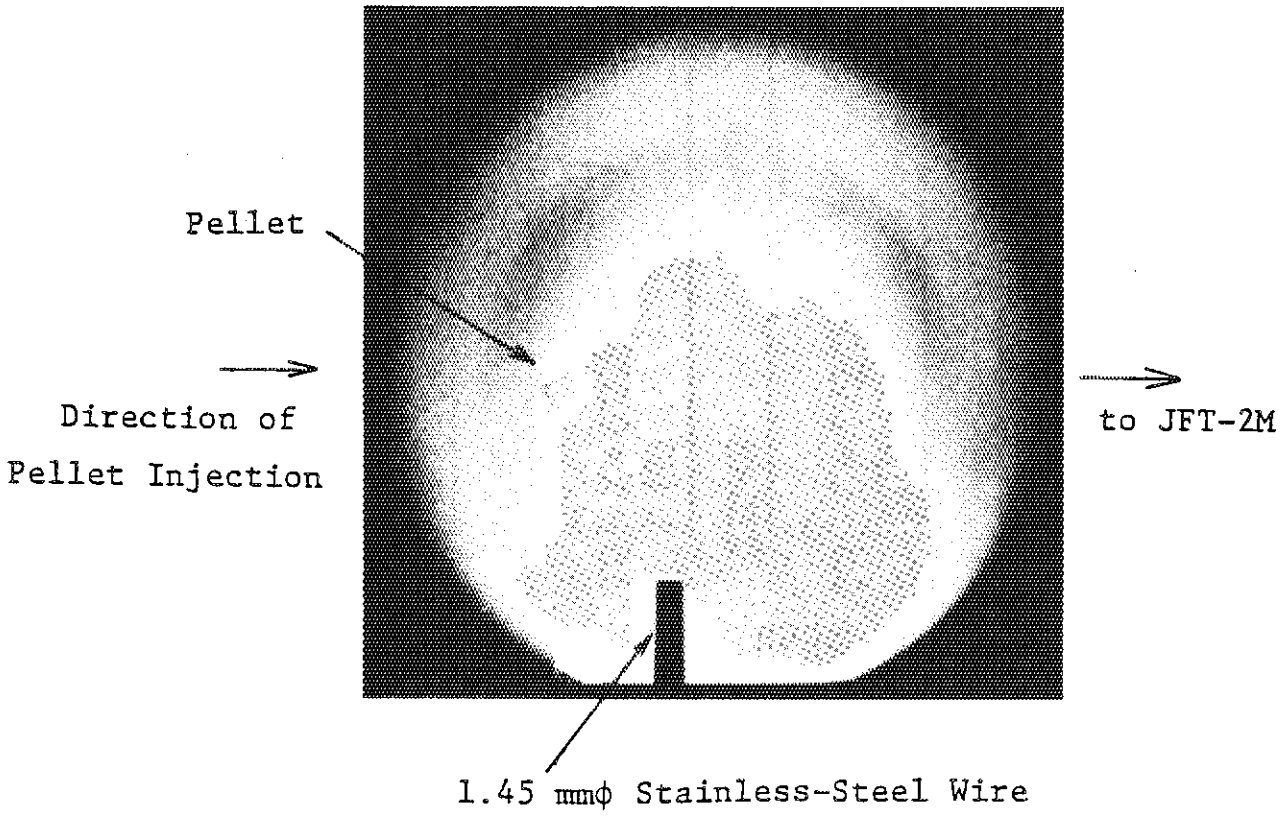

Fig. 13 Shadowgraph of D_2-pellet, pellet velocity = 769 m/s.

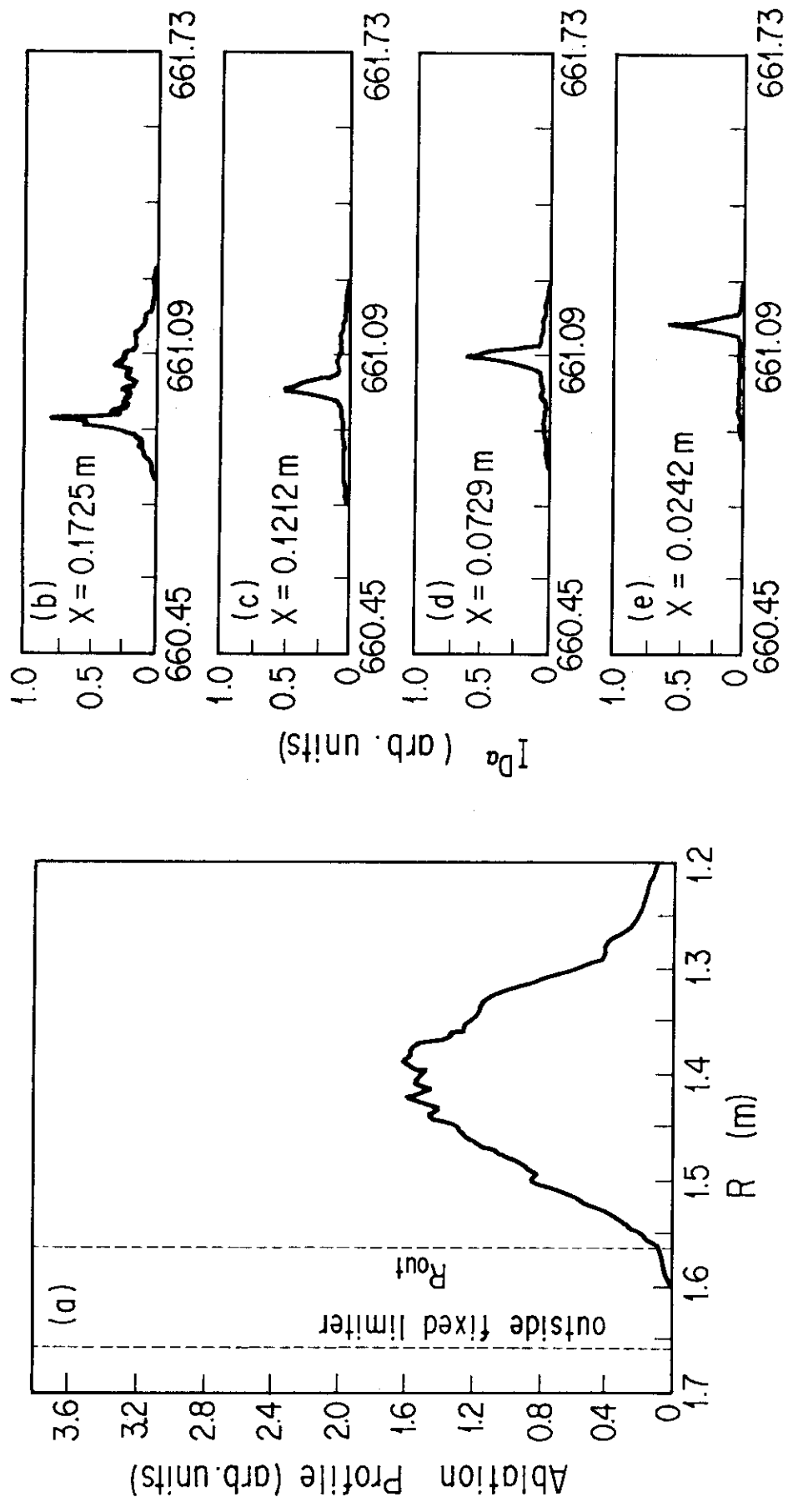

Fig. 14 (a) Ablation profile of D_2-pellet obtained by using 1 channel photo-diode, (b), (c), (d), (e) time histories of D_α line intensity at each channel of 8 channel photo-diode array.

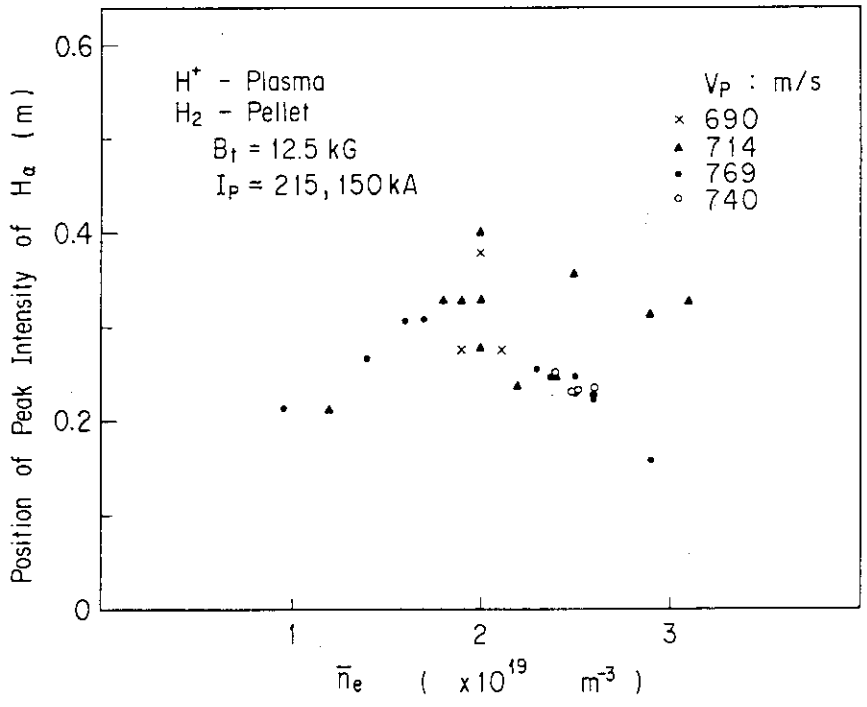

Fig. 15 Position of peak intensity of H_α line emission (peak deposition of particles) versus line averaged electron density. Ohmic heated discharges, pellet size = 1 mmϕ × 1 mmL.

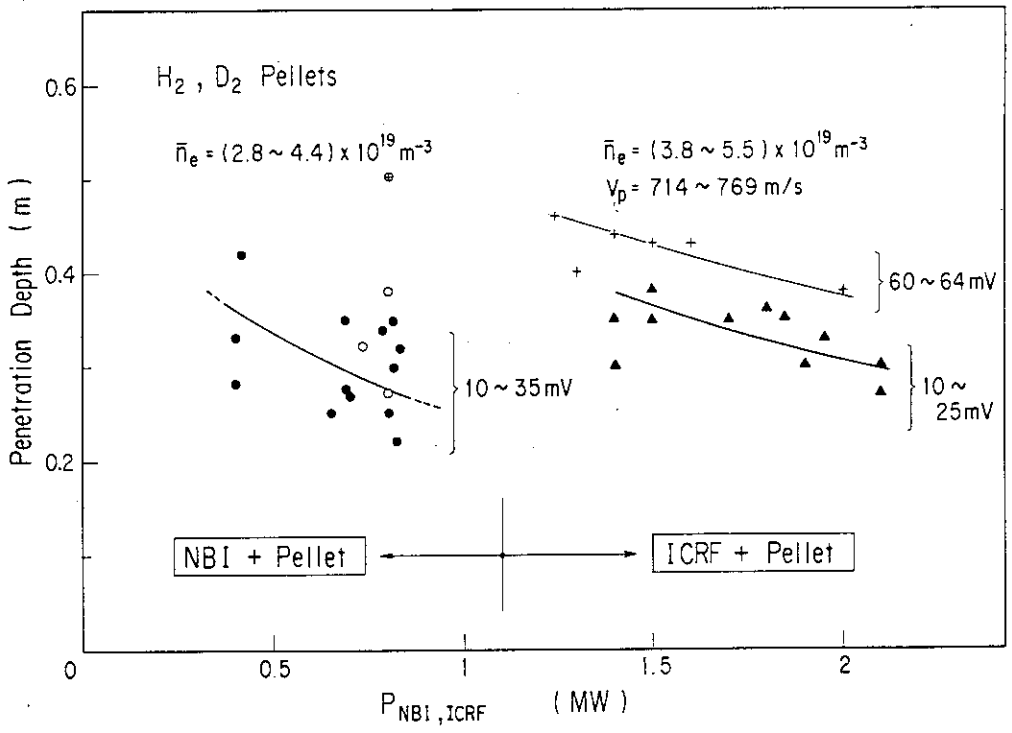

Fig. 16 Penetration depth of pellet (H_2 or D_2) in auxiliary-heated plasmas versus power of auxiliary heating, pellet size = 1.65 mmϕ × 1.65 mmL.

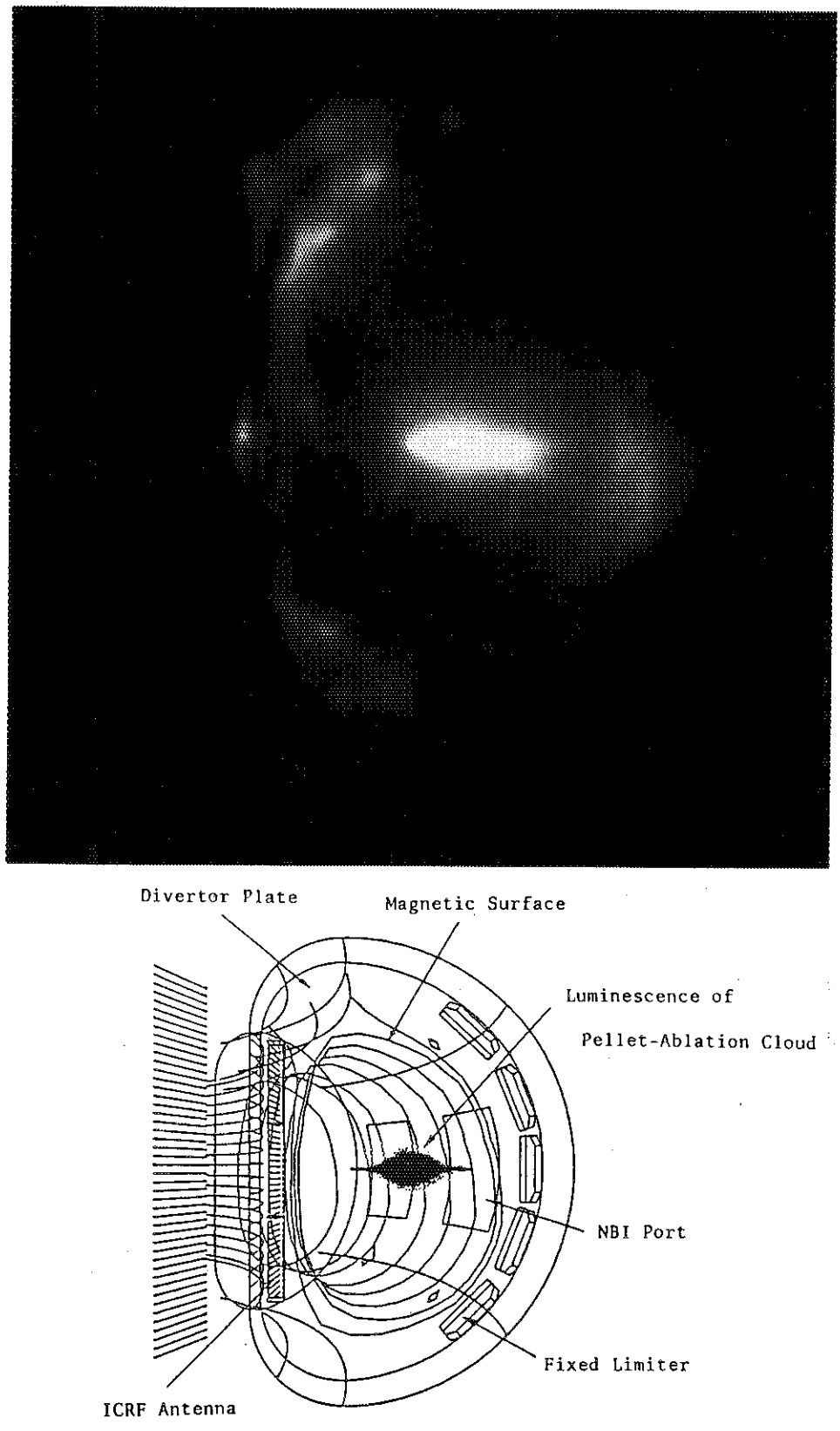

Fig. 17 Photograph of pellet (D_2) ablation (emission of D_α line) in upper single-null divertor discharges with NB (0.88 MW) heating. The pellet is injected from the direction of right hand side. $B_t = 1.3$ T, $I_p = 274$ kA, $V_p = 833$ m/s. The lower picture is three-dimensional expression of pellet ablation by the computer on the upper photograph.

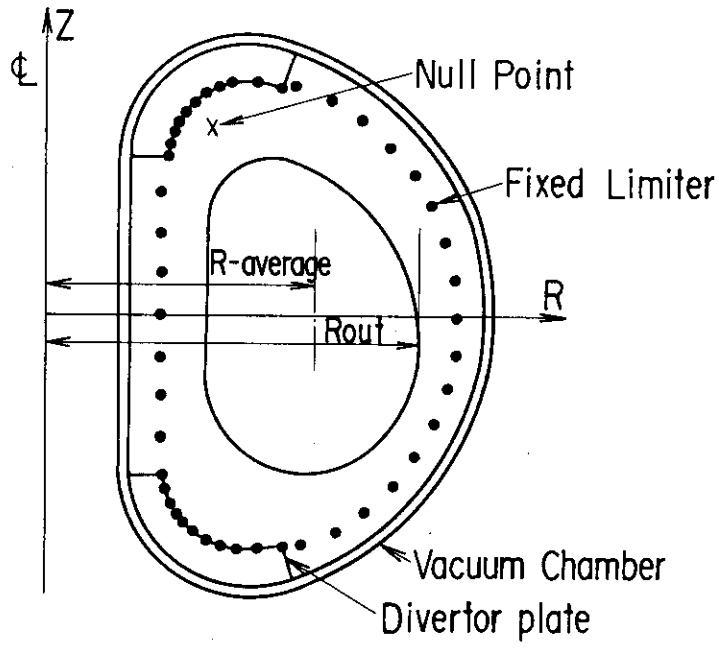

Fig. 18 Magnetic configuration in upper single-null divertor discharges with NB heating.

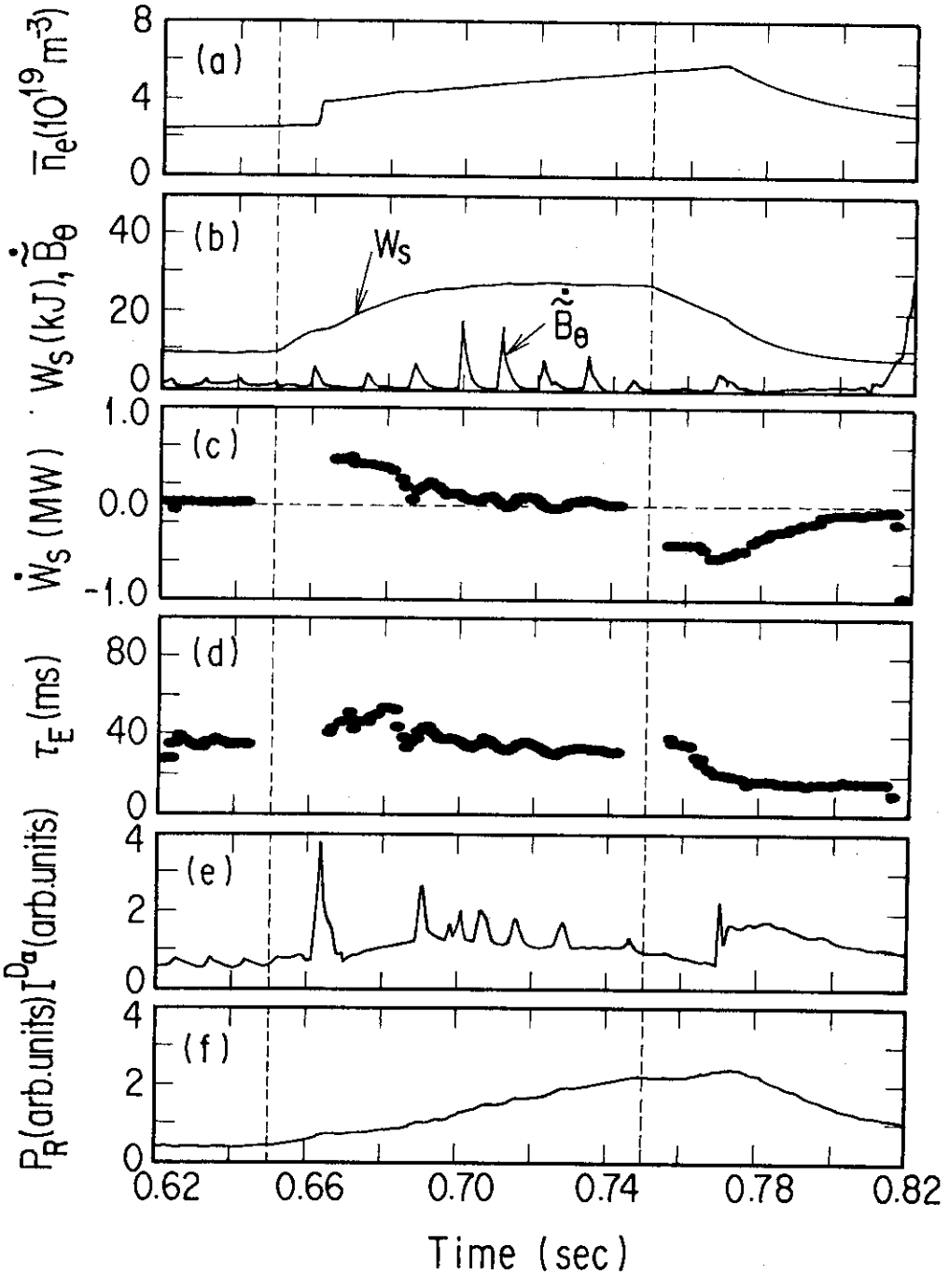

Fig. 19 Time evolutions of line averaged electron density ($\bar{n}_e$), plasma stored energy W_s, MHD oscillation signal ($\tilde{\dot{B}}_\theta$), time differential of W_s ($\dot{W}_s$), global energy confinement time (τ_E), intensity of D_α line emission ($I^{D\alpha}$) and radiation loss power including charge exchanged particle loss (P_R) in the single-null divertor discharges with neutral beam (NB) heating and small D_2-pellet injection ($\Delta\bar{n}_e = 2 \times 10^{19}$ m^{-3}).

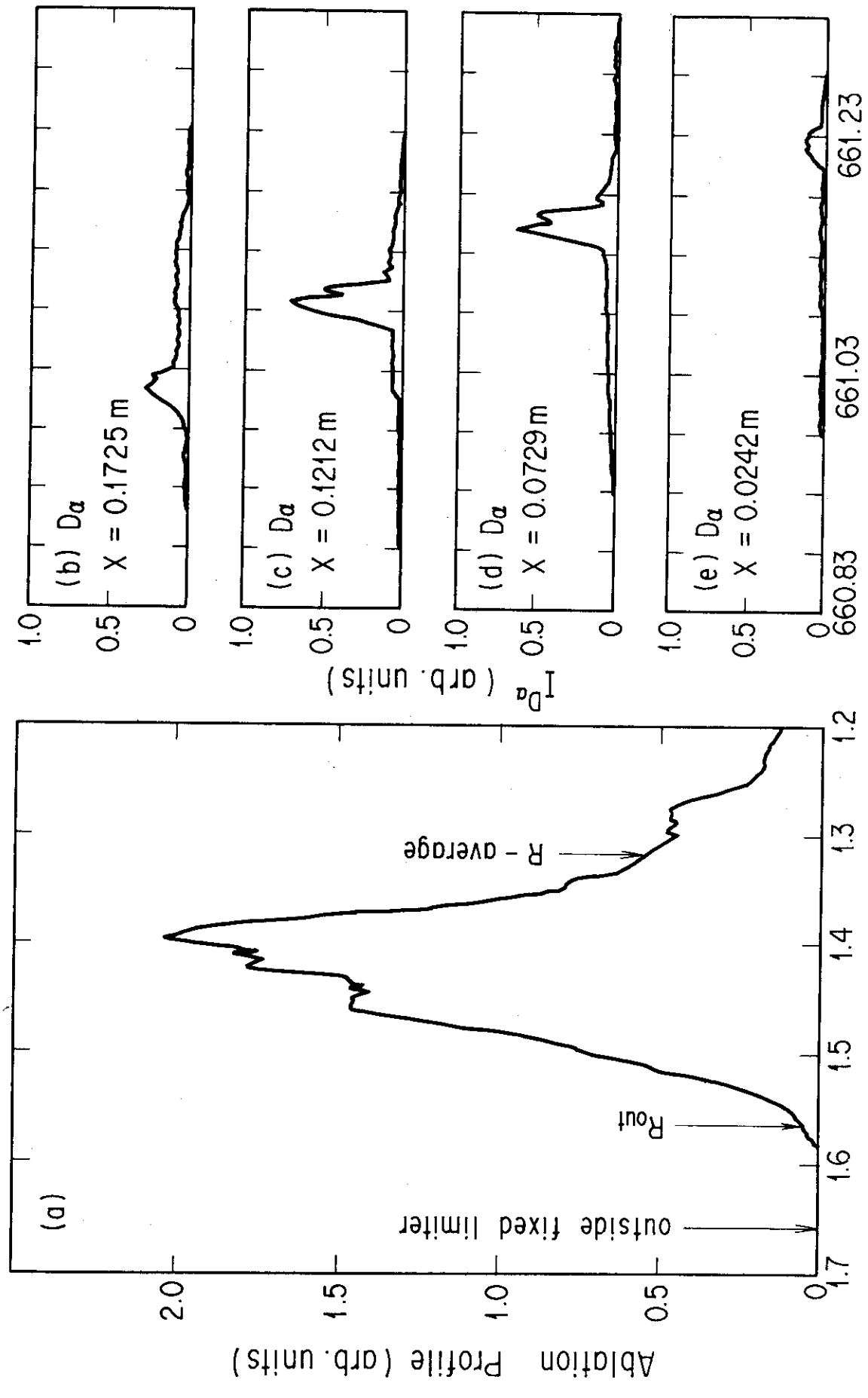

Fig. 20 (a) Ablation profile of D_2-pellet obtained by using 1 channel photo-diode, (b), (c), (d), (e) time histories of D_α line intensity at each channel of 8 channel photo-diode array on the discharges in Fig. 19.

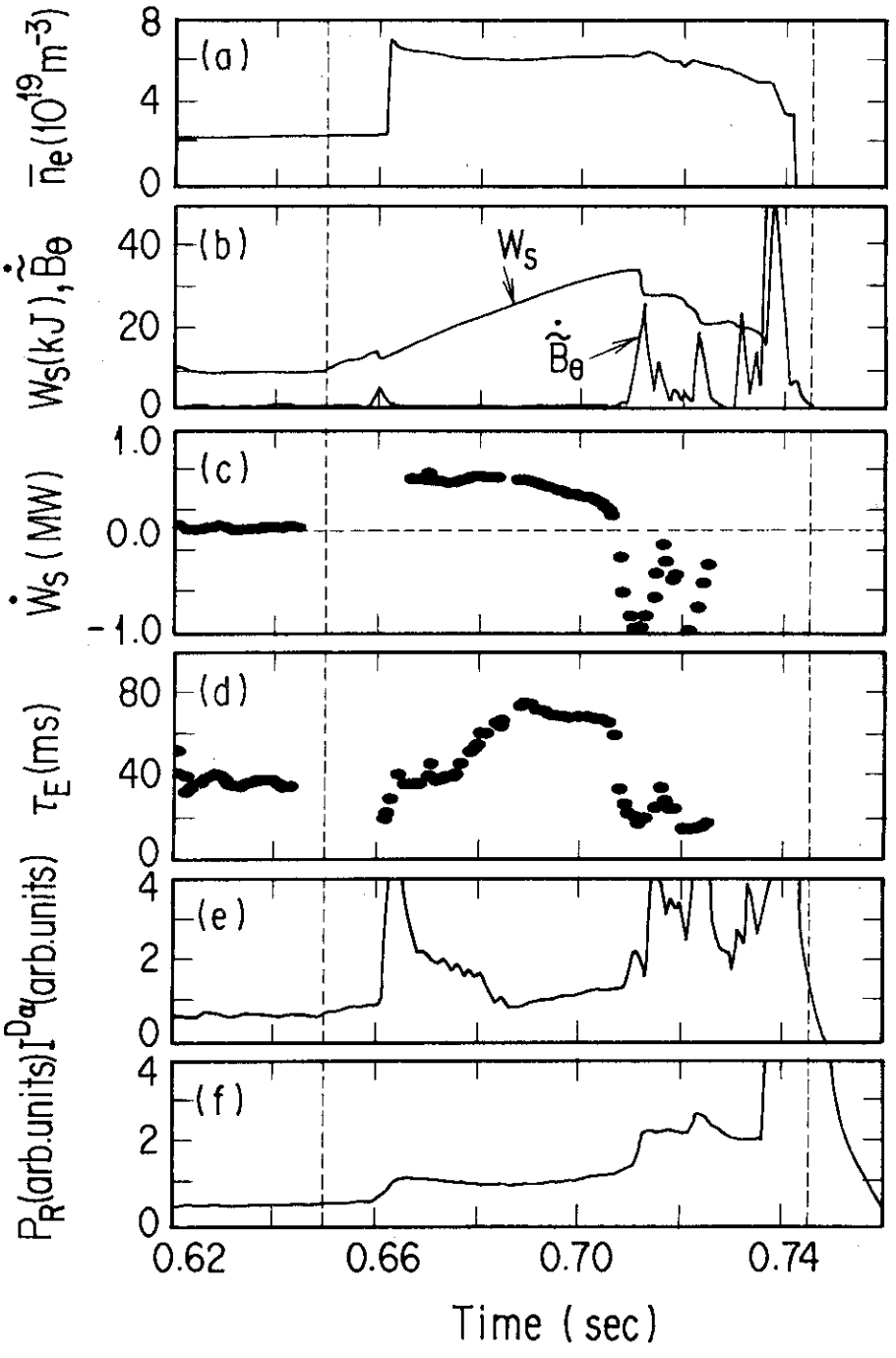

Fig. 21 Time evolutions of plasma parameters in the single-null divertor discharges with NB heating and large D_2-pellet injection ($\Delta\bar{n}_e = 4 \times 10^{19}$ m^{-3}) : columns from (a) to (e) are the same as Fig. 19.

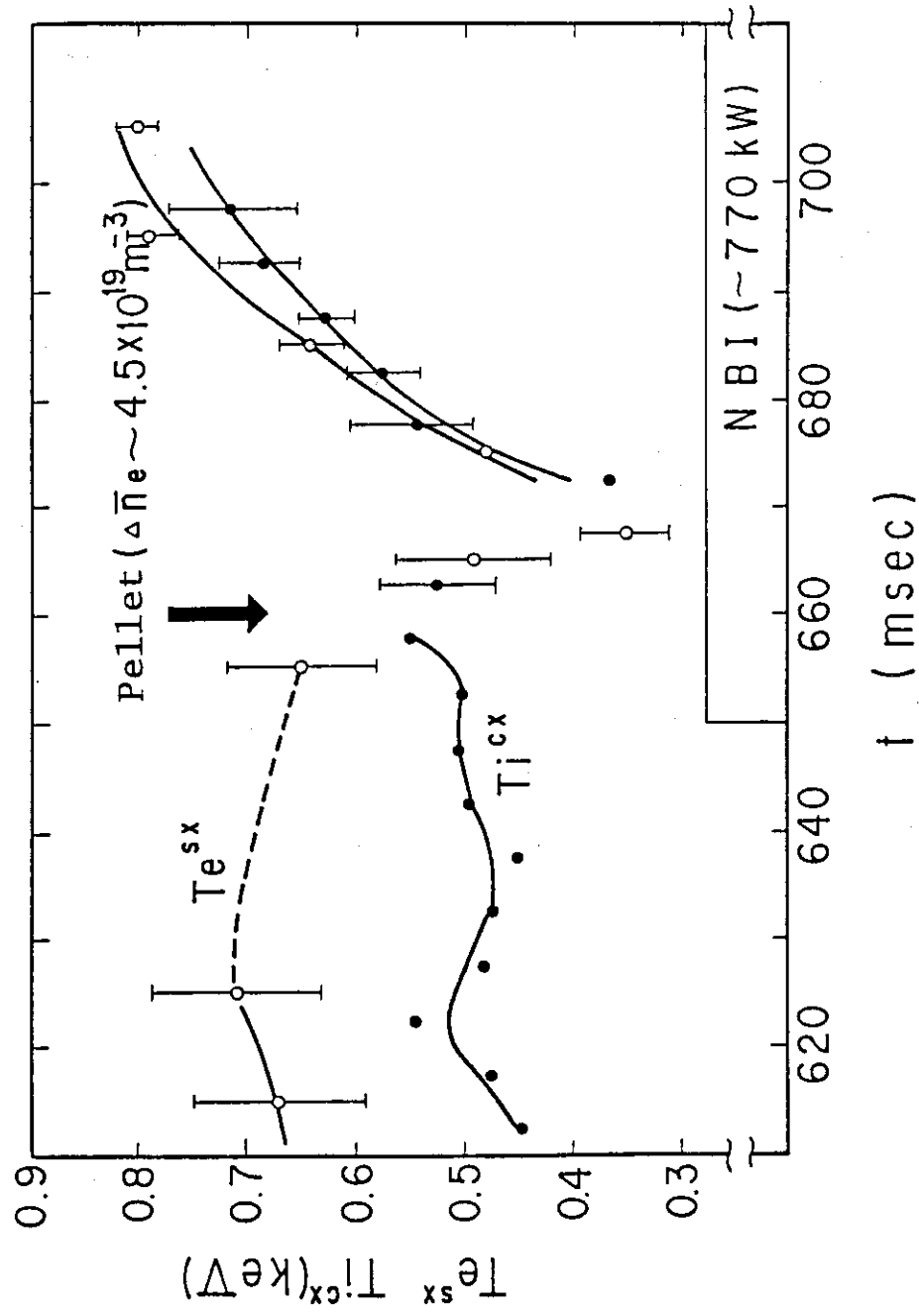

Fig. 22 Time evolution of electron temperature from soft X-ray analysis and ion temperature from charge exchanged neutral particle analysis in the large pellet injected discharges.

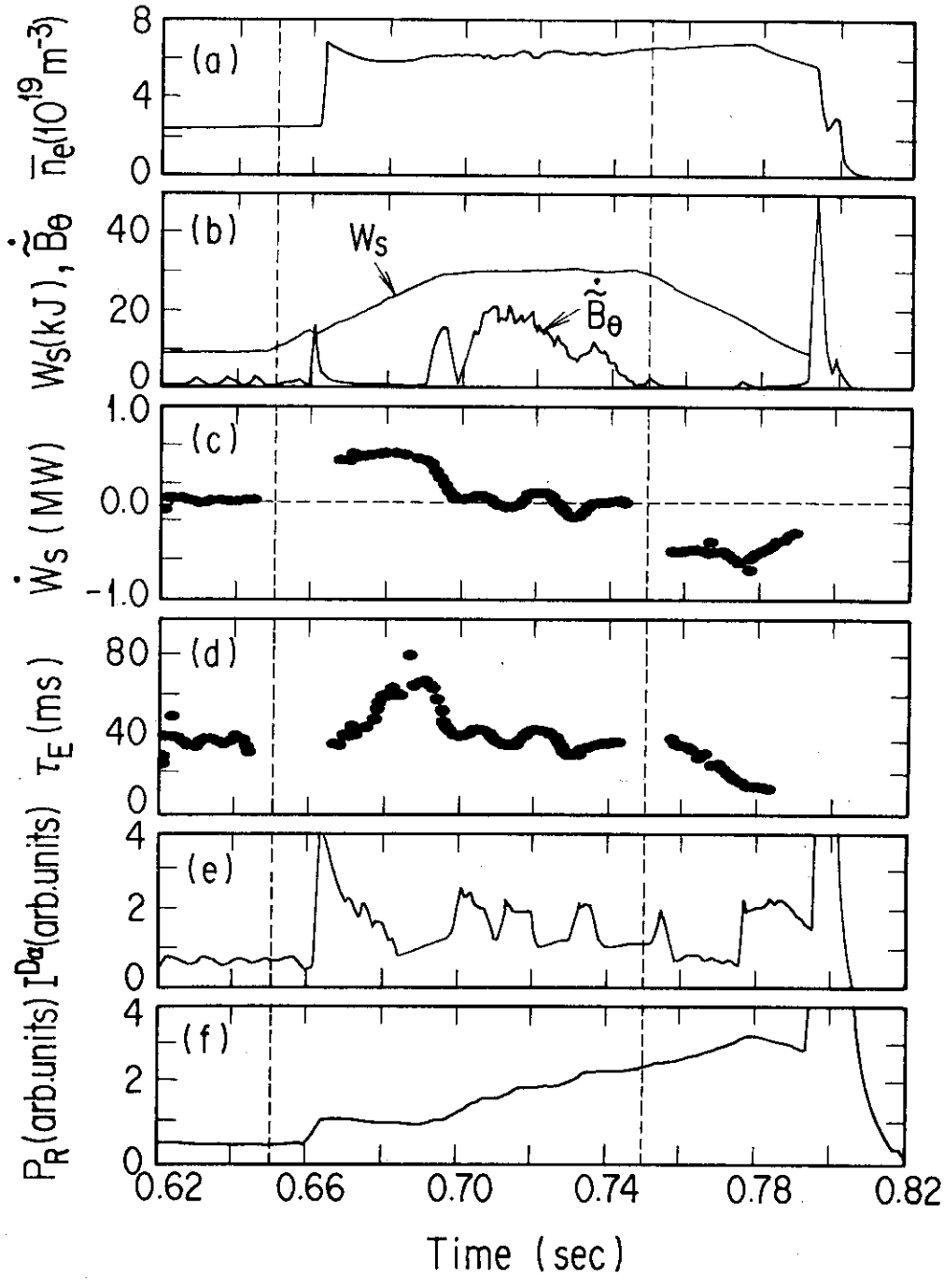

Fig. 23 Time evolutions of plasma parameters in the single-null divertor discharges with NB heating and large D_2-pellet injection ($\Delta\bar{n}_e = 4 \times 10^{19}$ m^{-3}) : columns from (a) to (e) are the same as Figs. 19 and 21.

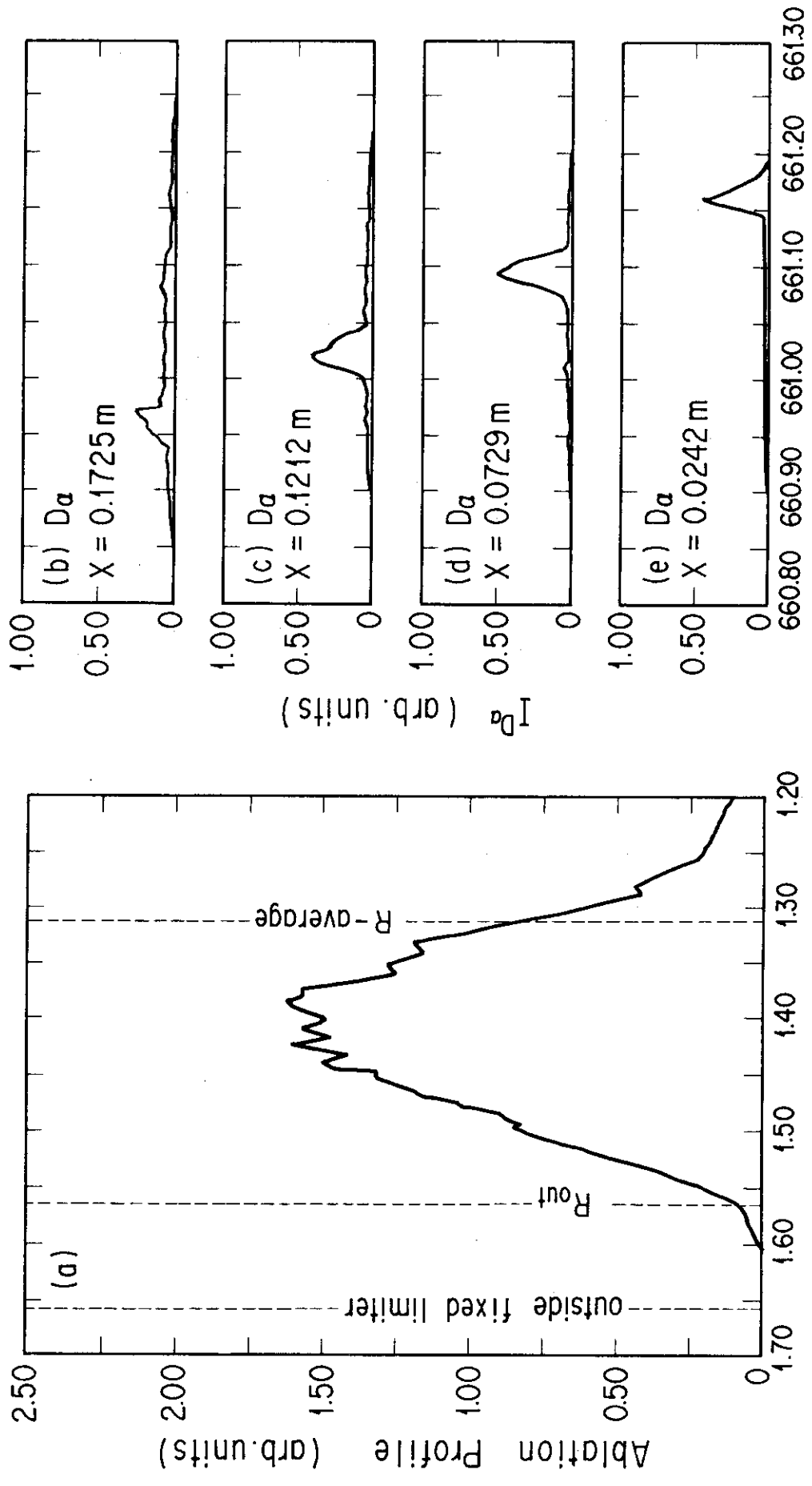

Fig. 24 (a) Ablation profile of D_2-pellet obtained by using 1 channel photo-diode, (b), (c), (d), (e) time evolutions of D_α line intensity at each channel of 8 channel photo-diode on the discharges in Fig. 23.

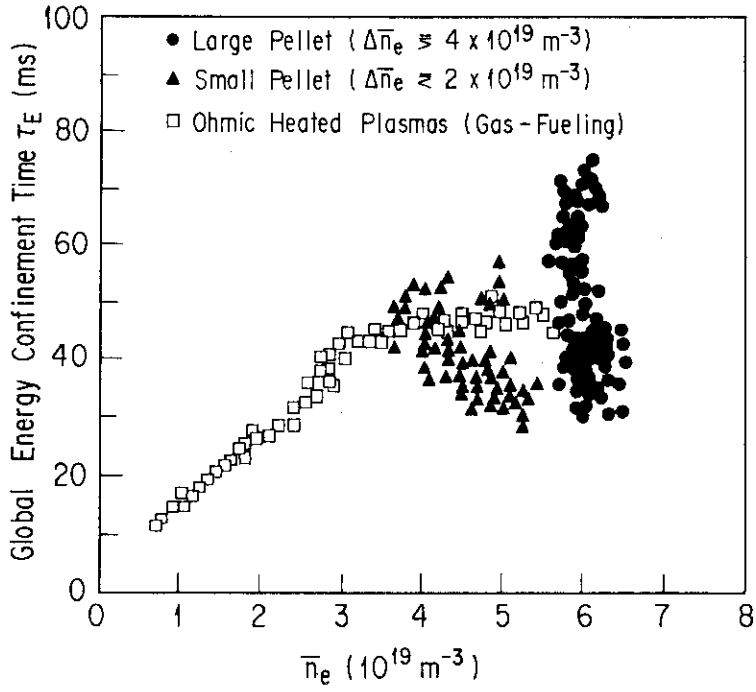

Fig. 25 Global energy confinement time versus line averaged electron density in the single-null divertor discharges with NB heating (pellet is injected into L-mode).

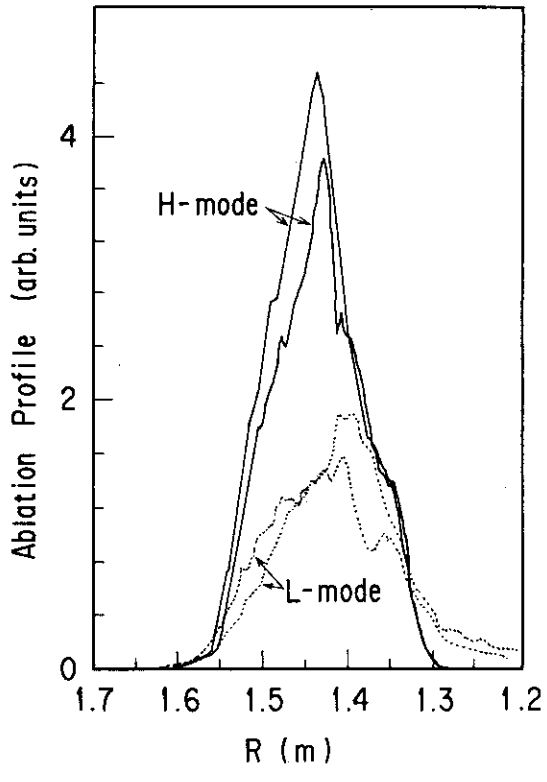

Fig. 26 Ablation profiles of D_2-pellet. Solid and dotted lines are profiles in pellet injection into H-mode and L-mode of the NB heated single-null divertor discharges.

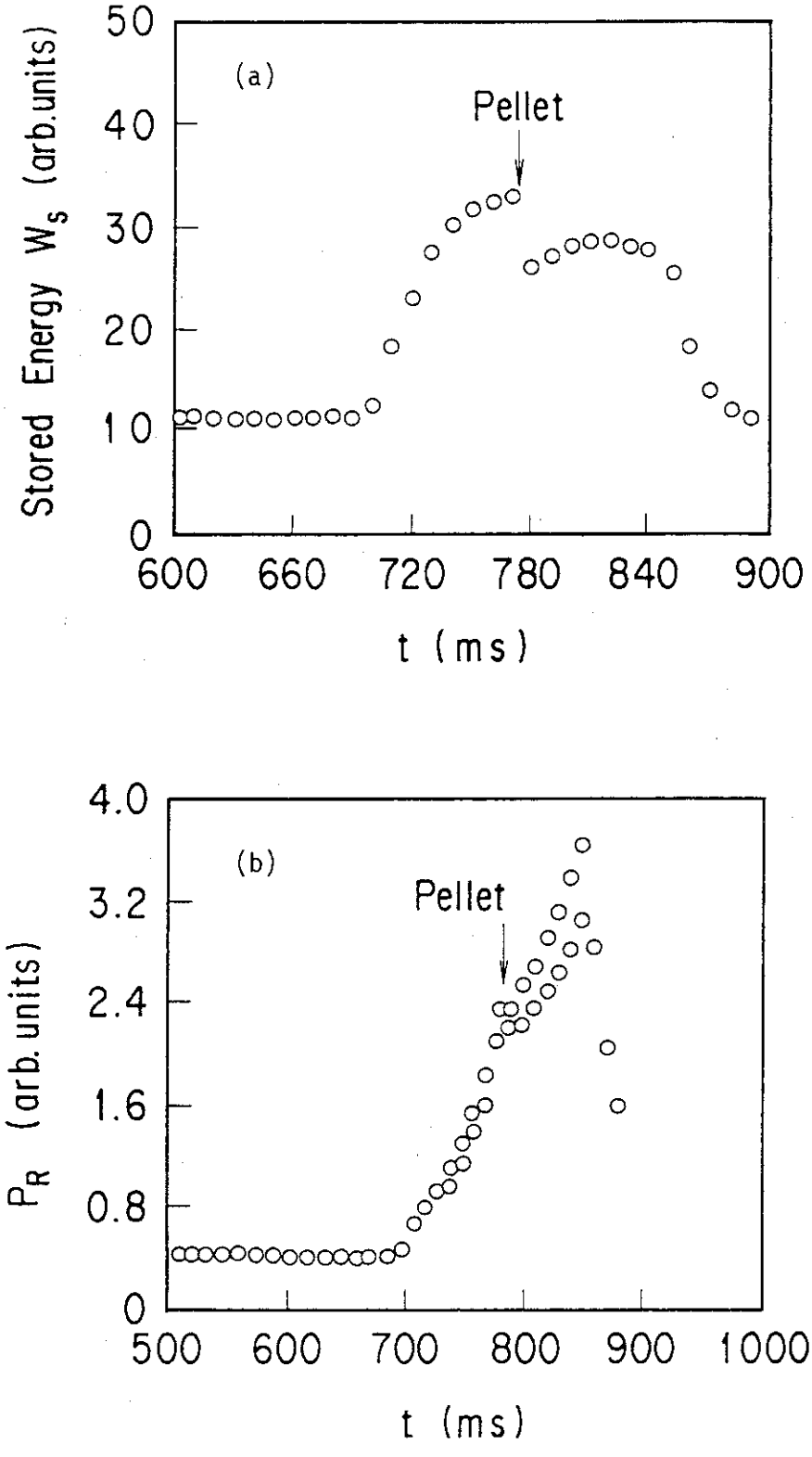

Fig. 27 (a) Time history of plasma stored energy (W_S), (b) time history of radiation loss power including charge exchanged particle loss (P_R) in pellet injection into H-mode of NB heated single-null divertor discharges.

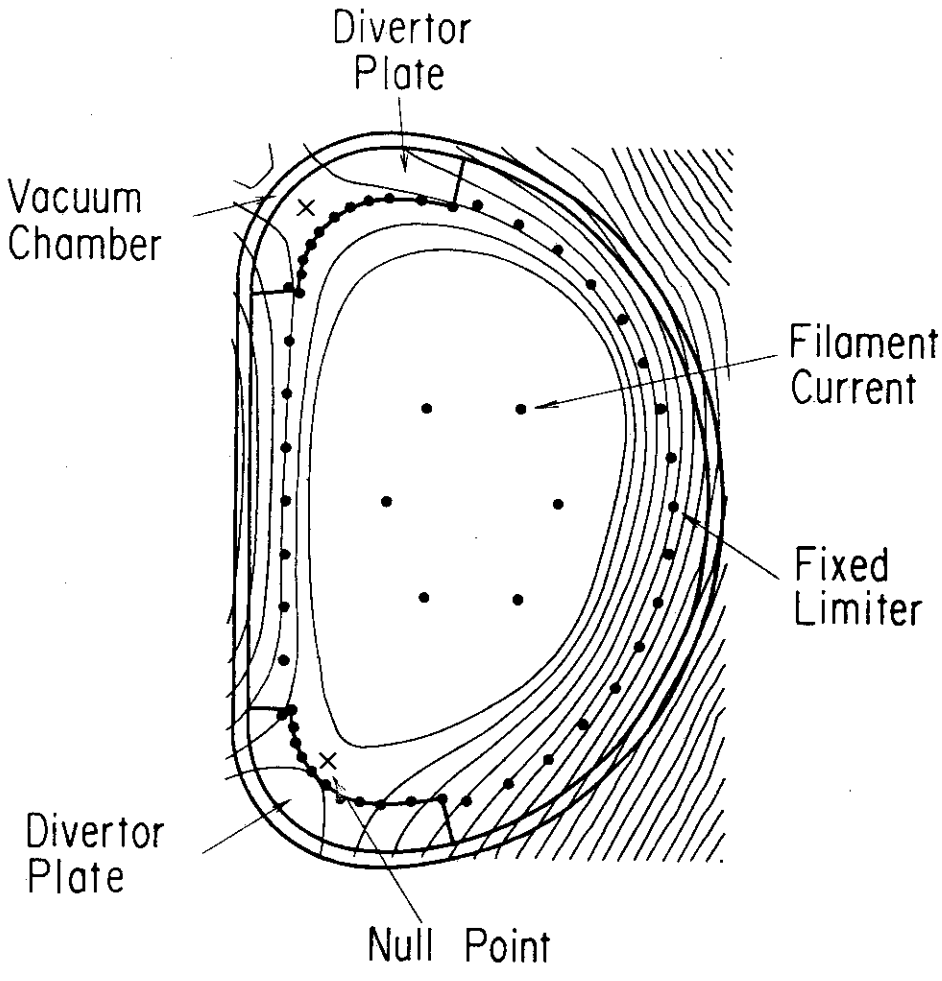

Fig. 28 Magnetic configuration in D_2-pellet injection into ICRF heated single-null divertor discharges.

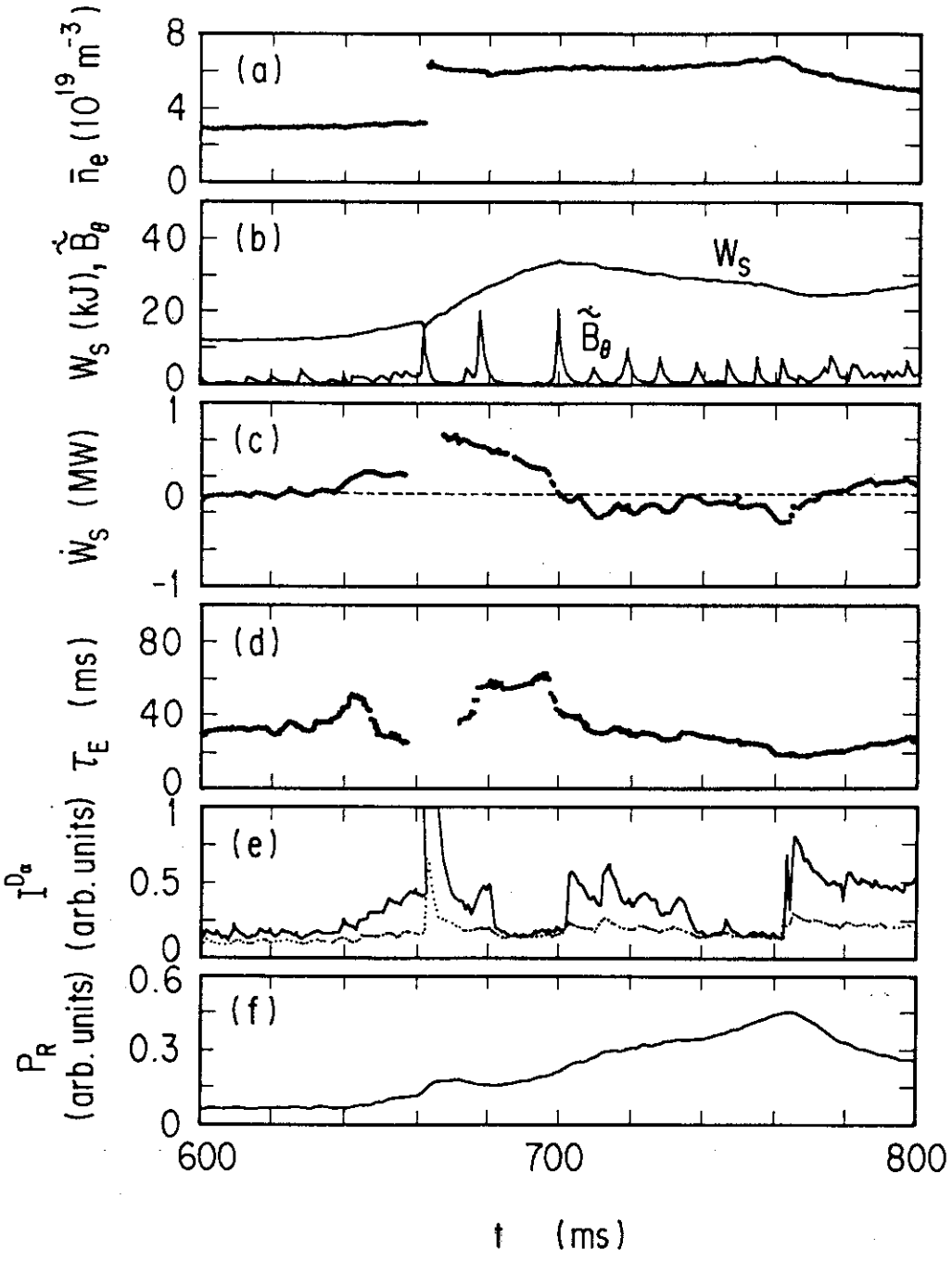

Fig. 29 Time evolutions of line averaged electron density ($\bar{n}_e$), plasma stored energy (W_S), Mirnov oscillation signal ($\tilde{B}_\theta$), time differential of W_S($\dot{W}_S$), global energy confinement time (τ_E), intensities of D_α line emission in the divertor (solid line) and main plasma (dotted line) regions ($I^{D\alpha}$), radiation loss power including charge exchanged particle loss (P_R) in the ICRF heated single-null divertor discharges. The pellet is injected into the L-mode at 660 ms and ICRF heating is from 600 to 900 ms.

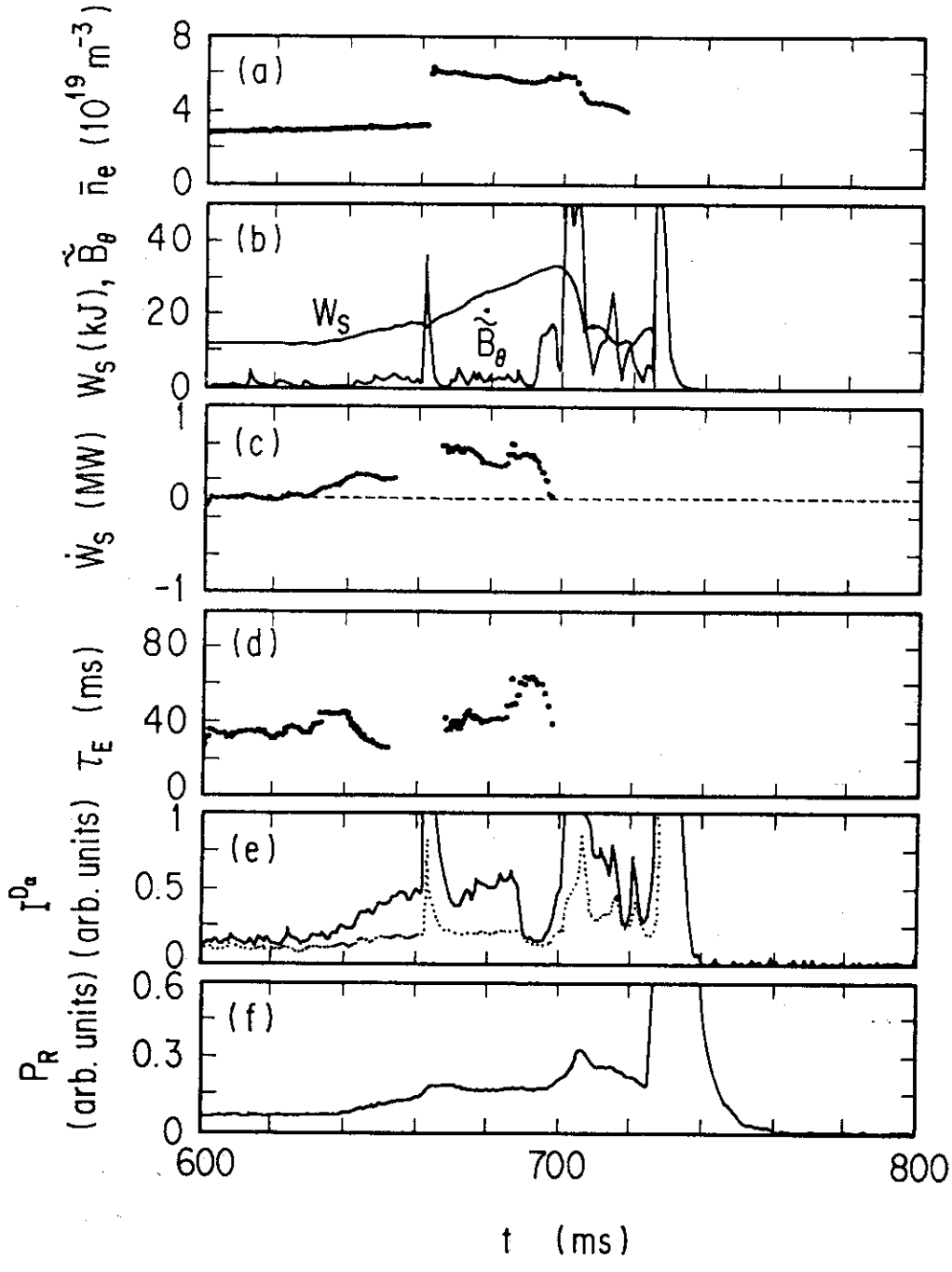

Fig. 30 Time evolutions of plasma parameters in ICRF heated single-null divertor discharges : columns are the same as Fig. 29. The pellet is injected into the L-mode at 660 ms.

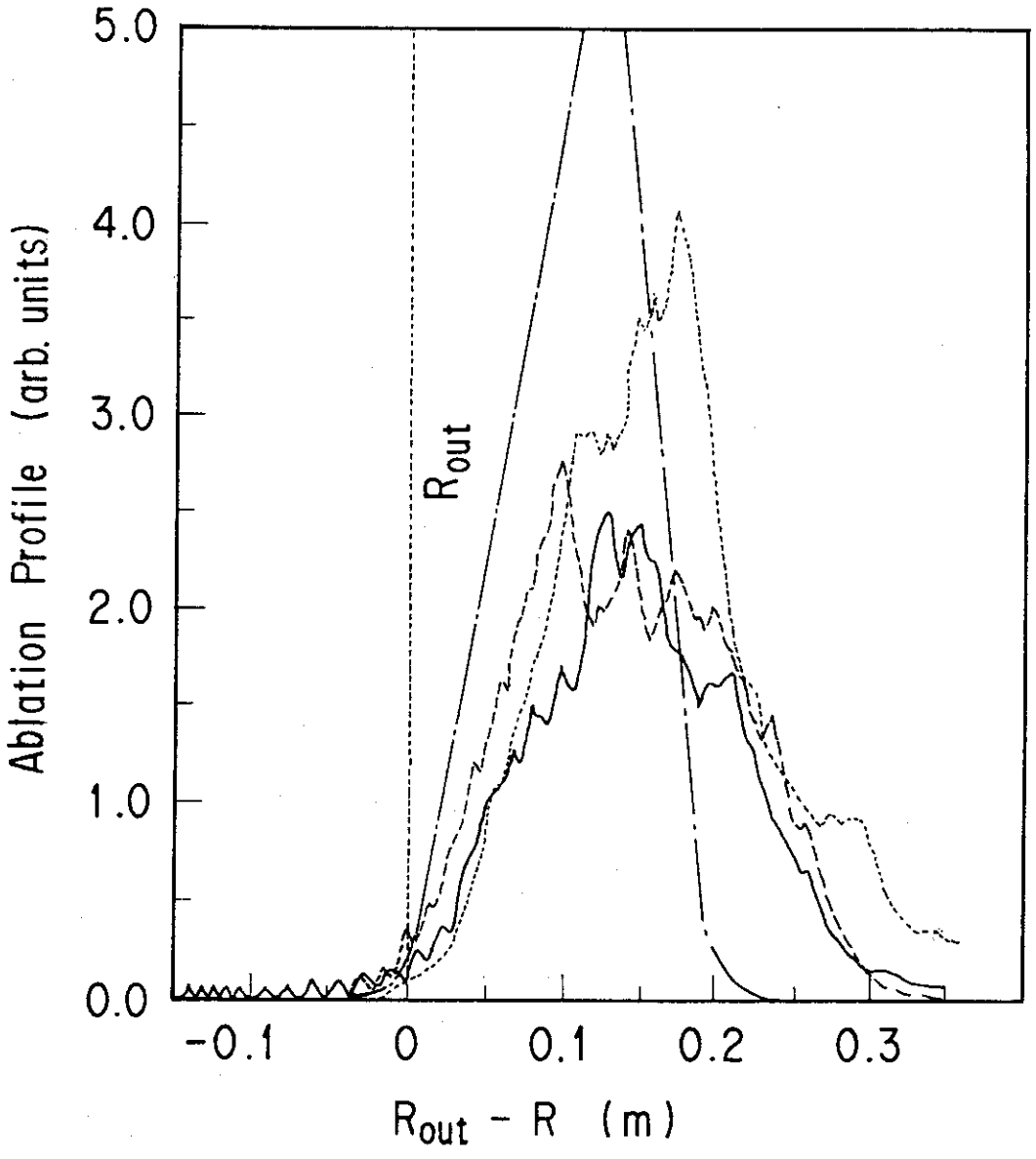

Fig. 31 Ablation profiles of D_2-pellet. Solid and broken lines are profiles in pellet injection into L-mode and H-mode of ICRF heated single-null divertor discharges, respectively. Dotted and dash-dotted lines are profiles in pellet injection into L-mode and H-mode of NB heated single-null divertor discharges.

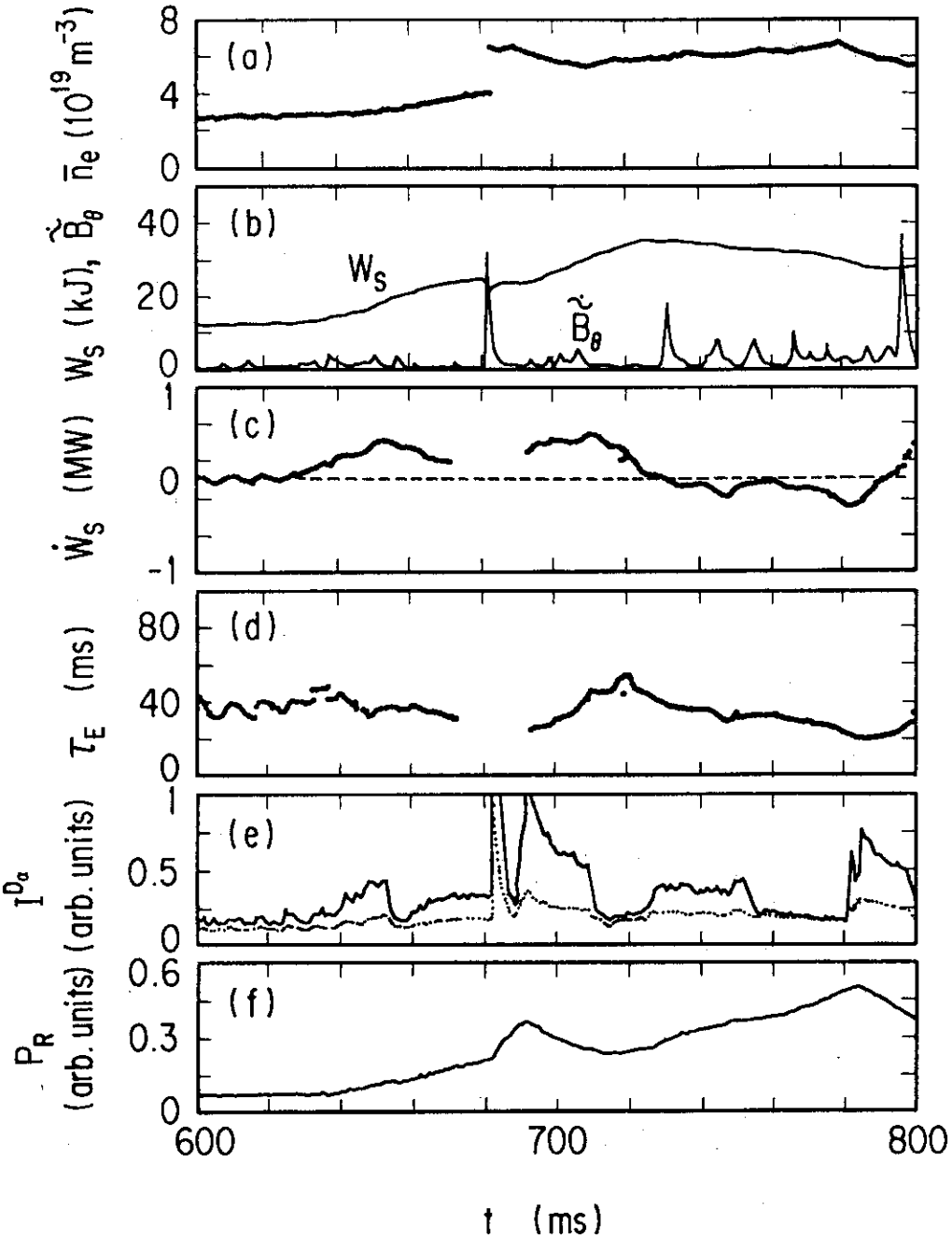

Fig. 32 Time evolutions of plasma parameters in D_2-pellet injection into the H-mode of ICRF heated single-null divertor discharges. Columns are the same as Figs. 29 and 30.

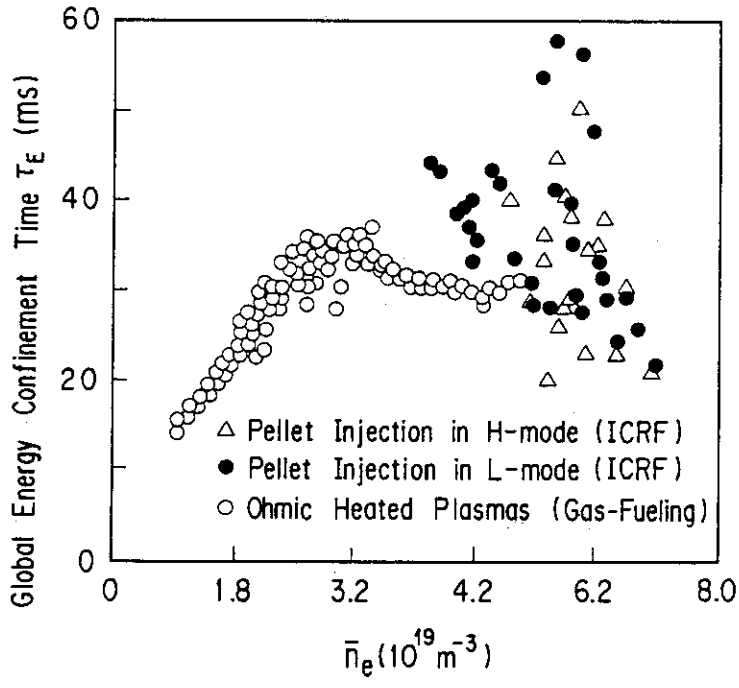

Fig. 33 Global energy confinement time versus line averaged electron density in ICRF heated single-null divertor discharges.

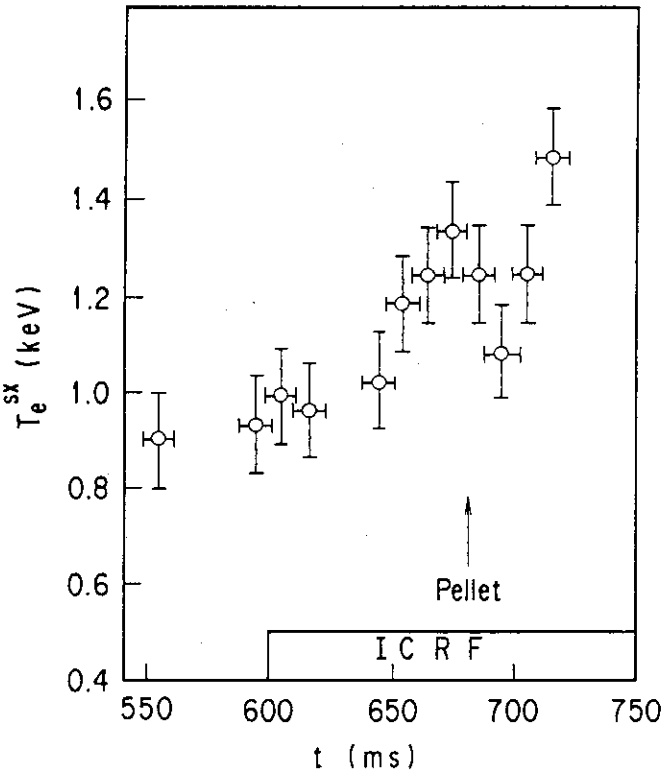

Fig. 34 Time evolution of electron temperature from soft X-ray analysis in D_2-pellet injection into the H-mode of ICRF heated single-null divertor discharges in Fig. 32.

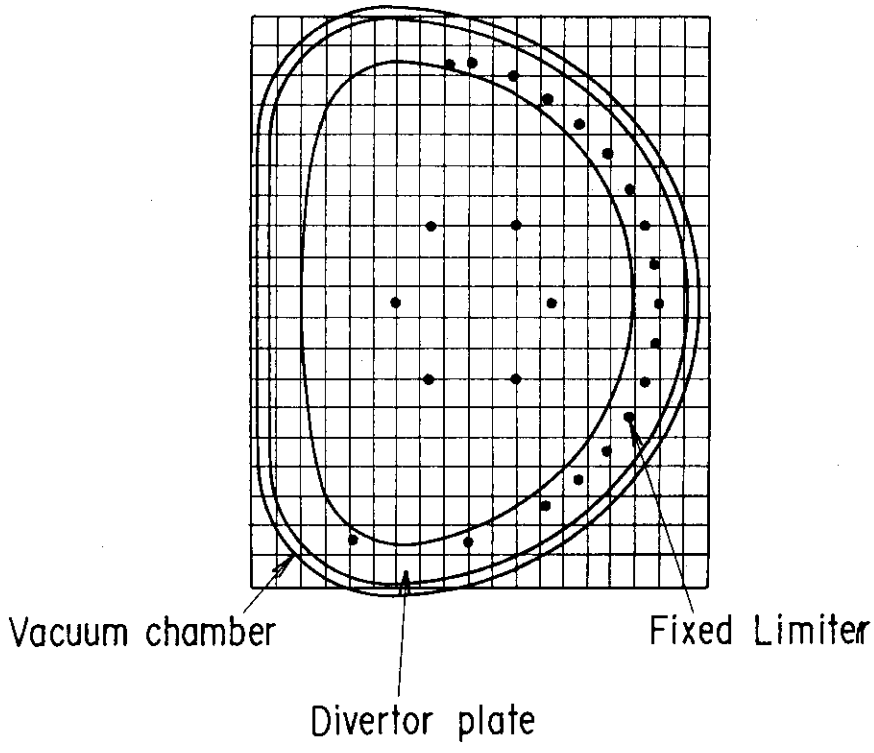

Fig. 35 Magnetic configuration in NB + ICRF heated limiter discharges with D_2-pellet injection.

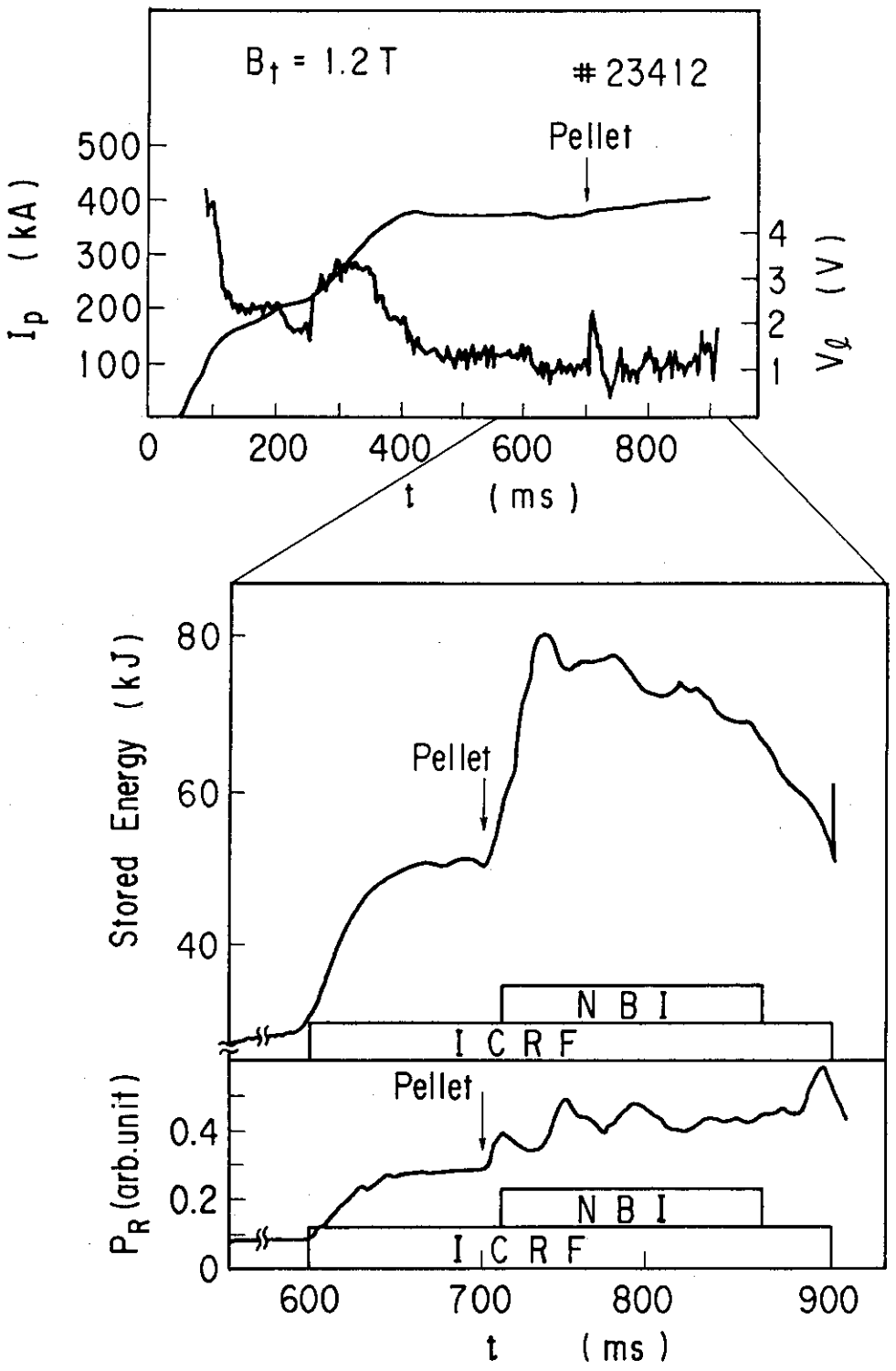

Fig. 36 Time evolution of plasma current (I_p), loop voltage (V_ℓ), plasma stored energy (W_s) and radiation loss power including charge exchanged particle loss (P_R) in D_2-pellet injection into NB + ICRF heated limiter discharges.

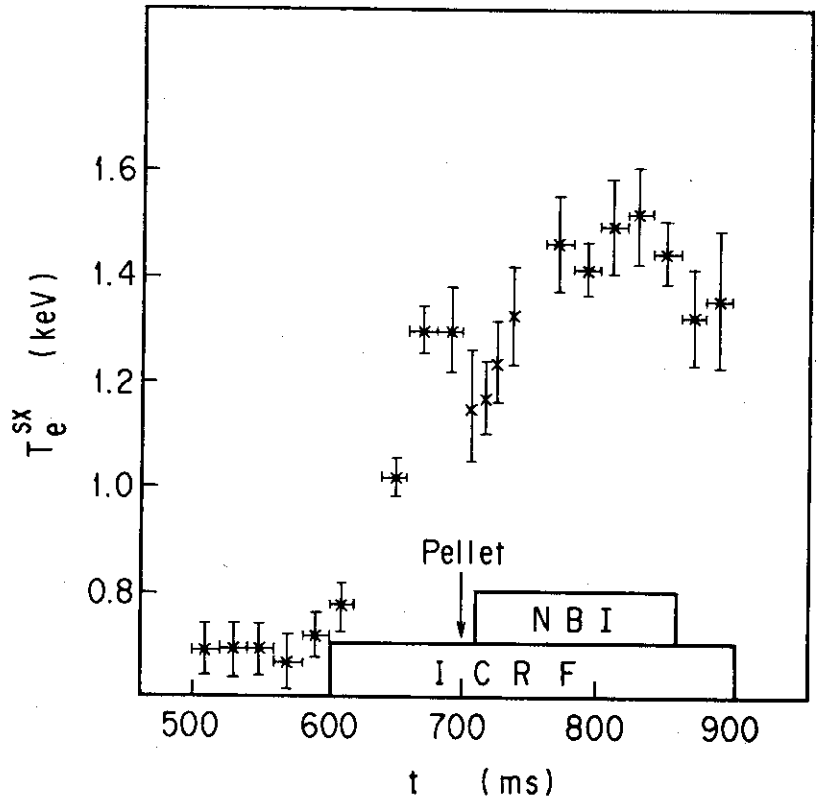

Fig. 37 Time evolutions of electron temperature from soft X-ray analysis on the discharges in Fig. 36.

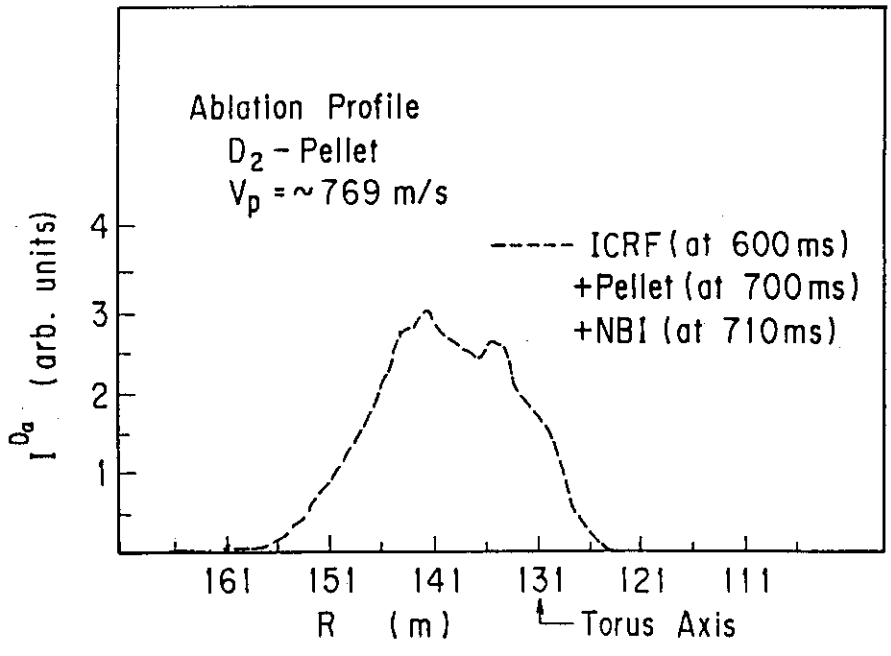

Fig. 38 Ablation profile of D_2-pellet on the discharges in Fig. 36.

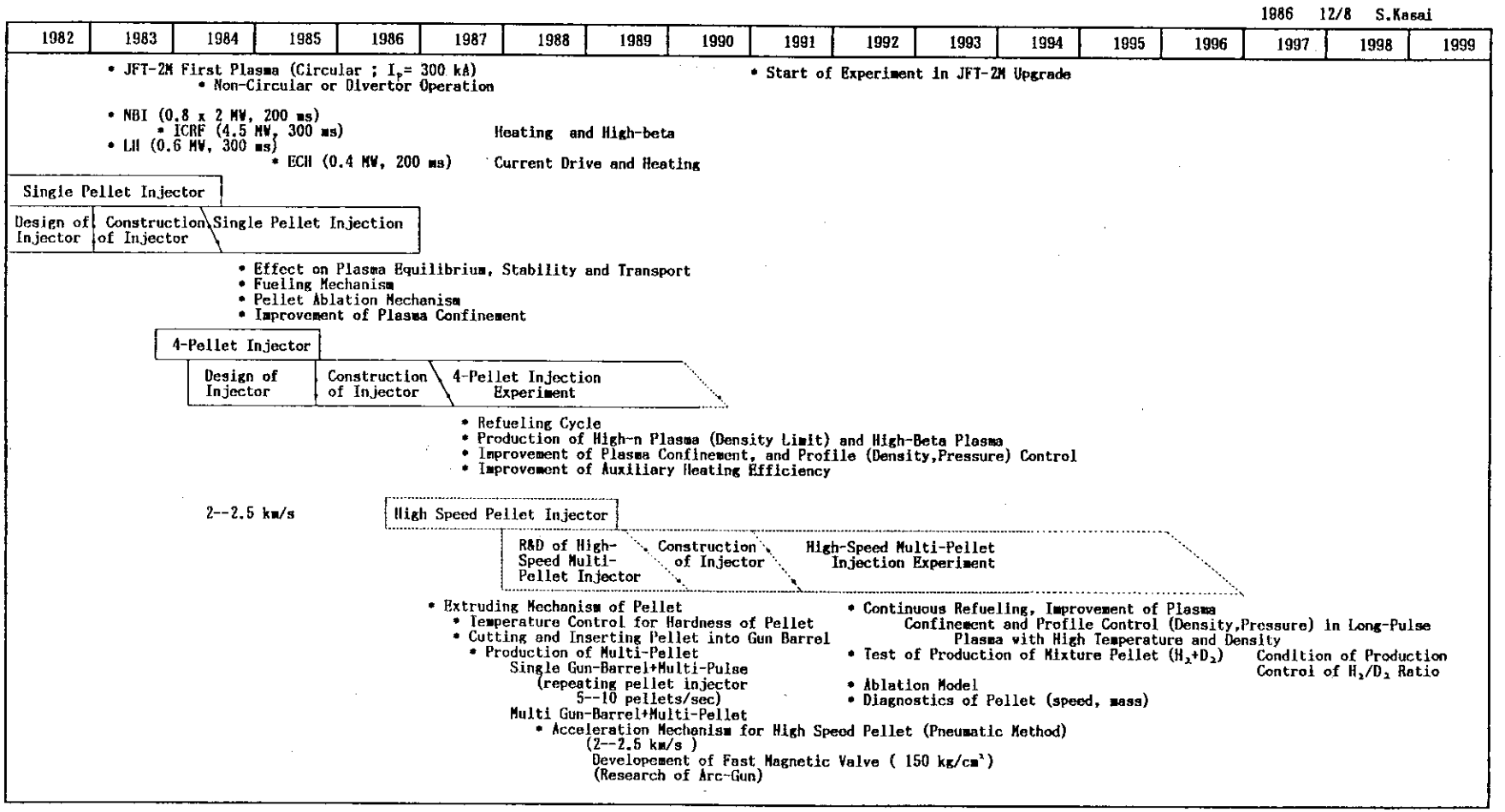

Fig. 39 Time schedule of development of the pellet injector and pellet injection experiment in Nuclear Fusion Research.

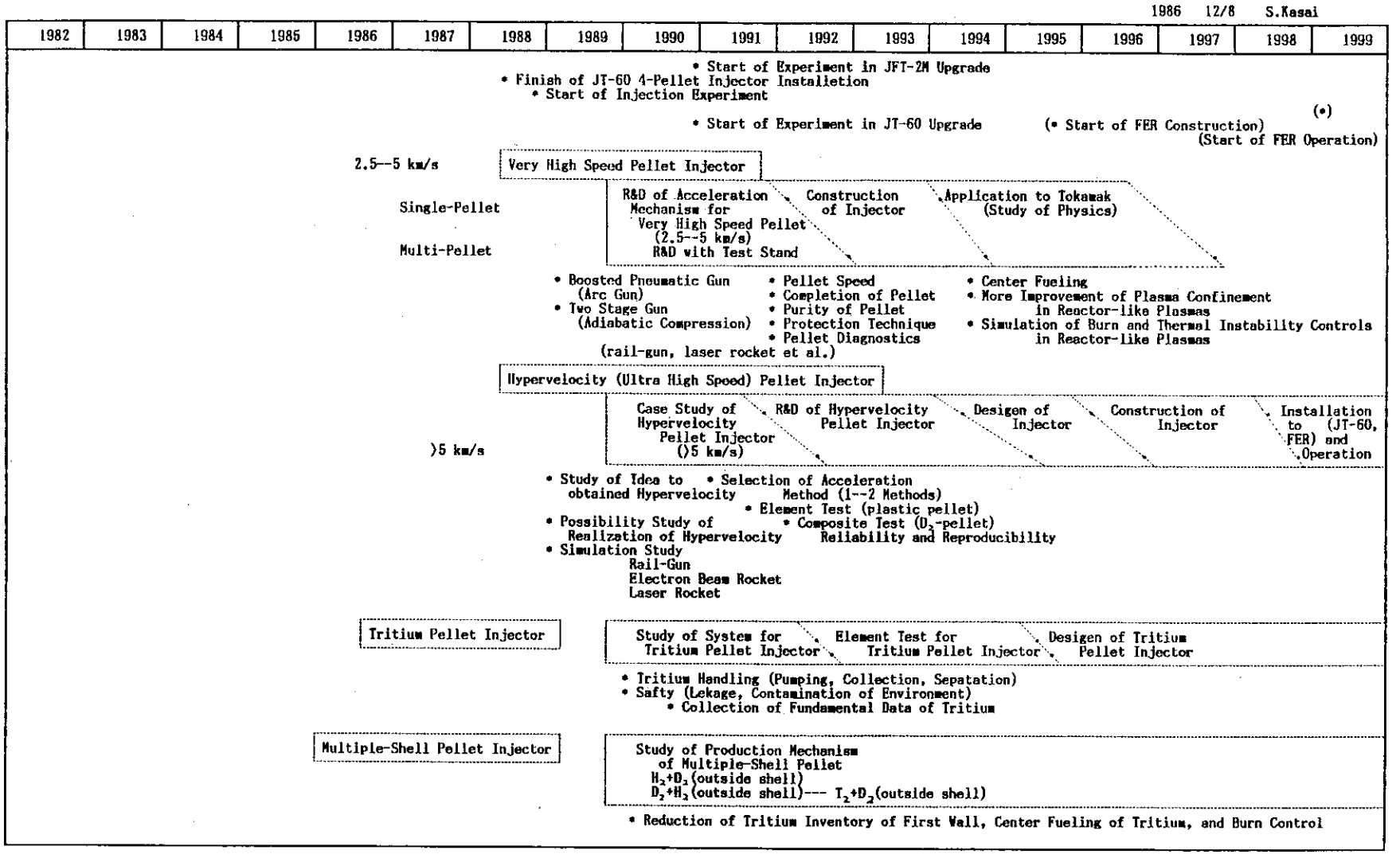

Fig. 39 Time schedule of development of the pellet injector and pellet injection experiment in Nuclear Fusion Research.